KfK 2822
Juni 1979

# PHAETON 2
# Flow Coast-Down Calculations Including Natural Convection In Helium Cooled Fast Reactors

D. Wilhelm
Institut für Neutronenphysik und Reaktortechnik
Projekt Schneller Brüter

Kernforschungszentrum Karlsruhe

KERNFORSCHUNGSZENTRUM KARLSRUHE

Institut für Neutronenphysik und Reaktortechnik
Projekt Schneller Brüter

KfK 2822

# PHAETON2 Flow Coast-Down Calculations Including Natural Convection in Helium Cooled Fast Reactors

D. Wilhelm

Kernforschungszentrum Karlsruhe GmbH, Karlsruhe

Kernforschungszentrum Karlsruhe GmbH
ISSN 0303-4003

## Abstract

Protected flow coast-down accidents calculated by the PHAETON2 computer code show that the shut-down heat of a gas-cooled Fast Breeder Reactor can be removed by natural convection in the primary loops. The differences in elevation needed for natural convection are feasible technically, because they are not greater than ten meters. From the calculations a number of criteria can be derived which should be taken into account in optimization of the primary loops.

PHAETON2 Durchsatzverlust-Rechnungen mit Naturkonvektion in heliumgekühlten schnellen Reaktoren

## Zusammenfassung

Die mit dem Rechenprogramm PHAETON2 analysierten Durchsatzverlustunfälle mit Schnellabschaltung zeigen die Möglichkeit, die Nachwärme eines gasgekühlten schnellen Brutreaktors mittels Naturkonvektion im Primärkreislauf abzuführen. Die dazu benötigten Höhenunterschiede sind technisch realisierbar, da sie nicht größer als zehn Meter sind. Aus den Rechnungen ergibt sich eine Anzahl von Kriterien, die bei der Optimierung eines Primärkreislaufes beachtet werden sollte.

Contents page

## 1. Introduction

During the last two years the main task of the PHAETON2 computer code was to analyse protected flow coast-down accidents in GCFRs with secondary steam cycles, taking into account either a back-up frequency of the helium blower or natural convection by a modified loop configuration. Before, the suitability of the code had been shown for transients with time constants higher than one second /1/.
Depressurisation accidents with time constants of several tenths of a second were calculated. Some first results of flow coast-down accidents have been published, as well. In /2/ the PHAETON2-code was described.
By a detailed model of the total primary helium loop and parts of the secondary steam loop the code solves the set of one-dimensional fluid dynamics equations together with the energy equations in the adjacent structures and machines and the point kinetics equation allowing for several feedbacks. A major option is that all boundary condition inputs can be changed with minor efforts so that, for example, different loop configurations can easily be modelled. Starting with the data of a 1ooo MWe design of KWU /8/ the code was used for several models, which are different in loop configurations, core design (for example hanging or standing), or in the degree of accuracy. During calculations, especially of flow coast-down accidents, the code of /2/ was improved substantially at those points, which are sensitive to natural convection effects and during flow reversal periods. The methods of solving the energy equations in the fluid with an analytical method inside a finite node, developed basically to match the point of flow reversal, proved to be helpful also in the transient calculations of the secondary loops. Four-quadrant circulator characteristics were not available, which is not a drawback, because it can be assumed in the code that the circulator runs down to zero frequency and stays there with a simple pressure drop correlation at standstill.

The driving force under that condition results from natural convection. Pressure drop characteristics of the primary loop at very low flow are results of only analytical work, thus, uncertainties in both circulator and loop flow resistances exist. The pressure drop in the core is always significantly higher, hence simplified correlations for the circulator are allowed.
To avoid major data substitutions the loops of the different configurations have been changed only in significant parts. Thus, designs might have been modelled, which are not optimised, but whose characteristics are not substantially different from that of the optimum. This does not include the design of the core, which may have a great influence on the natural convection potential, if one allows a variation in basic design characteristics. Only a small step in this direction has been made (see chapter 3.1) by introducing a new bundle with a 33 % increase in fluid cross sectional area. The potential of changing fluid dynamic capabilities by postponing the relevance of nuclear economy should be first examined in global parametric studies.
The results of PHAETON2-calculations can now indicate some major trends and concentrate the attention on some special safety related phenomena. After verifications of new designs, the code provides the possibility of proving expected results and pointing out special items worth further design efforts.

## 2. The model

To understand some of the peculiarities of the present results, a brief look at the computer model of the primary loop is presented. More details can be seen in /1/ and /2/.
The hydraulic model (see fig. 2.o) consists of plena, which are points representing large quantities of fluid mass with the same variables of state. At these points the energy exchange with the periphery is neglected. The plena are connected in an arbitrary way by links, which are lines of uniform mass flows. All links are subdivided by nodes, which are elements of uniform fluid properties. Inside the nodes the energy equation of the fluid is solved. The fluid exchanges energy with the adjacent structures. An energy balance is established inside these structures, as well as in the secondary loops and in the turbomachinery.

Because of the large variety of safety-related design features in GCFRs,it is impossible to calculate all the reference transients by a complex code, such as PHAETON2. Besides, transient characteristics of special components are often not available to the extent, necessary for the code input. Isolation valves, for example, are activated by a control system, which has not yet been modelled. If the valves are shut down, they impose very severe transients in the hydraulic network of the primary loops. This calls for very thorough knowledge of the shut-down characteristics in order to get realistic results of the whole hydraulic network. If necessary, computer runs have been performed with simplified characteristics, the results of which being a basis for further detailed examinations. But full-scale use has not been made of the code capacity, since a complex system with simplified boundary conditions has been modelled up to now. Further explanations of the input data being used are given in the discussions of the accidents.

## 3.1 The two core designs

Fig.1.0 shows the differences of two input files with which PHAETON2-calculations were performed. The old bundle design has a lower pressure drop but a better thermal performance of the two-dimensional roughness at the pin surface. The pressure drop and heat transfer correlations used with this bundle have been improved recently. In the new bundle, which has a broader roughness with a smaller thermal performance, direct measurements under thermal conditions are taken into account /3/. The new bundle which was fabricated also for irradiation tests at Mol, Belgium /4/ has a higher pitch of the triangular mesh of the bundle. The fluid cross section area and the hydraulic diameter increase substantially. Consequently, the pressure drop characteristic is better for the new bundle. To compare the low flow performances of both bundles, related Reynolds numbers must be assumed. With 3% mass flow and the nominal temperature rise of the core, the Reynolds numbers of the old and new bundles are 2980 and 3210, respectively. Thus, the Stanton numbers and Weisbach friction factors are very similar in both bundles. In the definition of the Weisbach friction factor a variation is presumed of the pressure drop which is proportional to the square of the mass flow per area, so that the resultant pressure drops of the new bundle are considerably lower than that of the old bundle. This is the major improvement during natural convection driven low flow for shutdown heat removal.
Fig.1.1 shows data of the new bundle steady state evaluation at the design point. For each of the 13 concentric subassembly rings, which are represented by 13 links, the fluid cross section area of the smooth part is given. Knowing the subassembly characteristics of the old bundle, changes are given in fig.1.1 by the new spanner width of the subassembly wall of 201.8 mm. To achieve outlet temperatures very close to the old design, orifices have been placed so that the total drag coefficient of a link can be read from the table. Here a constant value of 2.42 has been supposed for resistances at spacers. For link 7, the dynamic pressure is 19.2 kPa so

that the pressure drop due to the drag coefficient is 46 kPa. Calculating the pressure drop for a hypothetical link 7 with only smooth tubes, the value due to the Weisbach friction factor would be 91 kPa; then the difference of 163 kPa is only a consequence of the artificial roughness. At the interfaces between two enrichment zones non-steady steps can be read from the table as a result of the steps in the energy profile. In the radial blanket, which releases only a very small amount of energy, the orifices are closed to leave but a small passage. The mass flows are very small, and laminar conditions are found in links 18 and 19 with Reynolds numbers of 3170 and 3020, respectively. At these values the hypothetical nominal drag coefficient, which is given for fully turbulent flow, is supposed to be increased by 30%. By this the change from the turbulent law to the laminar one is taken into account, which constitutes a direct proportionality between the pressure drop and the fluid velocity. Actually in and near a highly closed orifice, laminar fluid laws are no longer valid, but to make calculations consistent, the mean undisturbed velocity is used as a reference. Thus, in link 19, a total of about 17000 dynamic pressures must be achieved for the pressure drop near and at the orifice, in order to reach the highly throttled flow. It is questionable whether such a reduced flow behaves similar to that of the centre core subassemblies without distortions in the velocity profiles, especially during low-flow conditions. Some answers are given for fig. 3.4. At the design point the high radial gradient of the amount of energy release in link 17 seems to be susceptible of causing major velocity distortions, but the Reynolds number in this link is 12800 so that turbulent exchange phenomena tend to smoothen high local gradients. There will be, though, a difference of velocities on the hot and cold sides of the subassembly but this is a local effect which does not devaluate the one-dimensional calculations of an average flow channel.

Fig. 1.2 shows some major input data for the present model.

### 3.2 Flow coast-down accident in a hanging core version with steam driven circulators

The model of fig.2.0 is used with the "new bundle" and a hanging core. Only one loop outside the reactor core is simulated, representing 8 parallel loops operated simultaneously. The reactor core consists of 13 concentric rings of subassemblies, the innermost being the center subassembly only. These rings are modelled by PHAETON2-links in which an average pin of the subassembly is connected to the one-dimensional flow channel between plenum P1 and plenum P2. The innermost links are numbered 7,8,9,10 and 11, and represent the first enrichment zone. Links 12 and 13 represent the second enrichment zone, links 14 and 15 the third, link 16 the fourth, and links 17,18 and 19 the radial blanket. The steam generators are elevated, so that the difference in height between the core center and the center of the steam generator is 10 m. The flow-coast-down accident starts at time=1s when all circulators loose power instantaneously. Normal scram activities are performed by inserting -7$ between time=2.15s and time=2.8s. The feedwater of the secondary loop is run down to a minimum of 3.7% proportional to the helium flow. The main turbine is bypassed and the pressures in the secondary loops are gradually reduced from 18700 kPa at the inlet and 7600 kPa at the outlet to 910 kPa and 370 kPa, respectively. This is an output of the present control activities in the secondary loops with the circulator turbine throttle valve being closed down to 6.6%. Any other activity is possible by a simple change of the code input.

The moment of inertia of the circulator and turbine is 33.4 $Js^2$ which is the five-fold value of the original steam turbine design. This value has been shown in the report /2/ (fig.18) to be necessary to avoid an instantaneous rise to very high cladding temperatures because with 6.7 $Js^2$ the normalized mass flow would nearly always be smaller than the normalized power generated in the core.

The friction momentum acting on the shaft is proportional to the 2.9th power of the frequency. With small frequencies, this would lead to very low deceleration rates of the shaft. With the steam driven circulator the shaft may be lubricated by water which enters the bearings at a tangential velocity, thus being able to drive the circulator. It has been stated in /2/ that the minimum blower frequency of 3.3 Hz is not sufficient to prevent the maximum cladding temperatures from reaching the point of failure, but with 5 Hz the maximum hot-spot is below 1100 K. Here, the lubrication is supposed to be of no help and the frequency runs down to zero, the friction moment being proportional to the 4th power of the frequency near standstill. Fig.2.1, 2.2, and 2.3 show the main output variables as functions of the problem time. The change from the 2.9th and 4th power, which is performed gradually produces a non-exponential change in frequency whose nature has a negligible influence on the temperature results. However the assumption that the friction momentum is constant would be more realistic (see fig. 3.1 ff).

At time=115s the frequency reaches 1 Hz and the impeller is supposed to transfer no more momentum to the fluid. The pressure in the outlet plenum of the circulator is still 1.8 kPa higher than in the inlet plenum (at that time the pressure in the upper plenum of the reactor core is 0.2 kPa lower than in the lower plenum the mass flow having reversed already). This effect can be observed if the circulator runs down not too slowly so that the fluid masses in the adjacent plena cannot be compensated. Although the mass flows revert first in the core links, the mass capacities near the circulator help the new flow direction to be initiated. This effect is stronger if the frequency gradient is high near circulator standstill and if the mass capacities are big in the adjacent plena of the circulator. A high frequency gradient near standstill is normally produced by a high friction momentum which leads to a rather early flow reversal. This is a drawback if one wants to avoid a high temperature rise in the upper reactor plenum because the core has no time to cool down and let the temperature in

the lower plenum fall to the design value of the upper plenum (550 K). As the natural convection driving force is proportional to the density difference in a simple model with only the reactor upper (index 1) and lower (index 2) plenum, and as the density difference is proportional to $(T_1-T_2)/T_1T_2$, the driving temperature difference must be the higher the greater the absolute values of both temperatures are. As long as the upper plenum temperature is lower than that of the lower plenum, the natural convection is not fully developed (cold chimney effect). It is thus desirable that flow reversal instantaneously leads to big negative mass flows in order to exchange the cold fluid in the upper core plenum. Here, both mass and heat capacity play a major role during the transient.

In addition to figs.2.1 to 2.3, fig.2.4 shows only the interval between time=99s and time=111s. The graph is constructed in a semi-logarithmic way, the ordinate being reflected at the abscissa, and a linear function being drawn for convenience. The results show oscillations which are supposed to be due to the discretisation methods of the PHAETON2 model. In link 18 (middle subassembly of radial blanket) these oscillations seem to be near the eigen-frequencies of the model but can be damped if new boundary conditions are reached (see the curve for negative mass flow). At the lower end of the figure the solid lines show when flow reversal occurs in the link considered. Link 17, which is the innermost subassembly of the radial blanket (zone 5), experiences the first flow reversal. The normalized shut-down heat generation in the blanket is at that time 5.8%; while the core region performs at 4.1%, the average helium density is 7.22 $kg/m^3$ in link 17 and 7.49 $kg/m^3$ in link 7. The Reynolds number of link 17 is 28 and that of link 7 is 630. The mass flow reverts a little bit earlier in link 17 because there the pressure of the helium column is slightly lower and the friction is almost the same as in link 7. The friction force is only 10% of the gravity force and the pressure in the lower plenum is already higher than in the upper plenum.

Fig.2.5 shows the axial temperature distribution in the fluid just before flow reversal starts (time=97 sec). The average temperature in link 17 is higher than in the rest of links considered. This leads to the fact already mentioned that the average density is the lowest of all core links. All links considered are heated up at time = 97 sec; thus the relatively big mass of the axial blanket zones tend to delay this procedure. The lower axial blanket even cools down the helium, the effect being greatest in link 7 where a rapid loss of flow in combination with the shut-down heat generation distorts the temperature profile considerably. It is thus the history of the preceding energy balances which causes link 17 to revert first. In link 19, which is subject to very low laminar flow already at the design point, the variation of the relative mass flow is not as great as in all adjacent links and the temperature profile is but little distorted. Similar explanations are given for fig.3.4.

The result could be changed by changing the friction in the links so that the sentive results are strongly influenced by the design differences between the core region and the radial blanket. Link 17 represents an average pin plus surrounding fluid annulus but the radial power variation is very strong here, so that the innermost pins are surrounded by a hotter gas giving rise to an even earlier flow reversal. This also could lead to flow recirculation inside the subassembly but this only can happen as long as the driving pressure difference between the adjacent plena is sufficiently low. Once the flow reversal is initiated, hot helium enters from the lower plenum, thus helping to reduce the gravity force of the helium column. Therefore, the time to reach significantly lower gradients of the negative mass flow is smaller than expected by linear extrapolation from the positive mass flow phase.

Furthermore, the results show that flow reversal continues in the center of the core, then moves step by step to the core periphery with small discontinuities at the boundaries of the enrichment zones because there the power level changes stepwise. Link 18 with its great oscillations reverts three times

and then comes back to positive mass flows for 1.5s before reverting definitively.

The sum of all mass flows of links 7 to 19 becomes negative together with the third enrichment zone. Subsequently it helps to reduce the cold chimney effect of the outer helium loops. The steam generators are no more counterflow heat exchangers, so that a highly different temperature profile must be established. The mass of the iron structure is ten times higher than that of the $H_2O$ so that it takes a long time to reach quasi-steady values. In the meantime, high axial temperature gradients occur in He and $H_2O$, the helium performing at first with increasing and decreasing temperatures in each steam generator. The calculation has been stopped long before a new temperature profile has developed.

The cladding temperatures of the radial blanket vary but little with time because of the relatively high heat capacity of the structure material adjacent to a relatively low helium mass flow. Comparing link 7 (innermost core subassembly) with link 17 (innermost row of radial blanket subassemblies) we find link 7 to have 525 kg mass of iron and pellet structure and 10.3 kg/s of helium mass flow at the design point; the data for link 17 are 37425 kg and 55.8 kg/s. Dividing the product of structural mass and heat capacity by the product of helium mass flow and helium heat capacity, we find a first approximation to the time constant for the energy to be removed from the structural material without taking into account nuclear production. For the mass flows at the design point this leads to a time constant of 3.4s in link 7 and of 45s in link 17. With typical values for mass flows during natural convection phase (time=240s), the time constants grow to 120s in link 7 and 2460s in link 17. Here, the mass flows in the radial blanket are rather small (1.8% of the design value) compared to the core region (2.9% of the design value) because the cladding temperatures are low, and so are the helium temperatures, giving a bad performance of natural convection. Following the explanation of the report /2/, page 57, the mass flows decrease very similarly in all links but at the design point link 17 already a near laminar flow prevails (Re=12800).

During the first 10s the heat transfer coefficient of link 17 is reduced by 85% whereas that of link 7 is only reduced by 65%. Therefore, the heat generated in link 17 which is relatively higher than that in the core region, cannot be carried off as well as in link 7. Consequently, the temperatures rise in link 17 and fall in link 7.

After time=10s the Nusselt number still falls in link 7 while a constant laminar Nusselt number of the radial blanket has been reached (Nu=5.3) and the heat transfer coefficient of the blanket is 0.32 kW/($m^2$K) which is 17% of the design value. The mass flows are no longer proportional in the core and blanket regions when natural convection is the main driving phenomenon. When flow reversal occurs in the radial blanket, the upper region of the pin which is still at low temperatures cools down the helium. This leads to an increase in helium and clad temperatures in the lower part and a decrease in the upper part. The temperature maximum moves but slowly from the lower to the upper part because of the relatively big heat capacities. At time=240s the exit helium temperature is still 610K (545K at the design point).

The core region undergoes such a temperature distortion too, but it takes only about two minutes to constitute a new monotonous helium temperature distribution. Up to time=230s, the cladding of the upper axial blanket is at such low temperatures that is cools down the helium. This is by far the last region to reach the new steady temperature level because of its low heat generation, the big mass, and the extreme temperature rise to the new exit value.

There are two maxima for the hot-spot cladding temperature, the first being a function of the zone of inflection of the nominal cladding temperature at time=140s. With a strongly increasing upper plenum temperature at that time the natural convection becomes so strong that the temperatures in the core tend to be stopped from increasing which has a negative influence on the driving natural convection. The negative mass flow overshoots a little and then gets balanced at a quasi-steady value.

## 3.3 Flow coast-down accident in a hanging core version with electric motors driving the circulators

The model of fig.3.0 is used with the "new bundle" and a hanging 13-link-core. The steam generators are elevated. Again, all circulators loose power at time=1s and a shut-down takes place between time=2.15s and time=2.8s by insertion of -7$ (see fig.3.1). The momentum of inertia of the circulator/motor system is 330 $Js^2$ which is a value for an electric motor driving a two-stage circulator. To avoid major changes in PHAETON2, the circulator characteristics of a steam driven circulator with 216 Hz design frequency have still been used. Thus, the friction momentum has been set constant at 1180 J which is 10% of the motor momentum at the design point to reach zero flow at time=190s. The feed water of the secondary loops is run down proportional to the square of the helium flow because with the low helium flow gradient in the beginning proportional running down would lead to filling the whole secondary loop with water. The main turbine is bypassed and the circulator turbine throttle valve is closed down to 6.6%. After 2 minutes the pressures of $H_2O$ have reached a quasi-steady value with 840 kPa at the inlet and 340 kPa at the outlet of the model. Compared to the heat generation in the core, the frequency of the circulator is high for the first 180s, the result being a steep decrease of all temperatures except that of the lower reactor plenum which is fed by helium leaving the steam generator (see fig.3.2). Even the cladding temperatures in the radial blanket decrease significantly, showing the great delay by the heat capacity of the structural material adjacent to a relatively low helium mass flow. By great mass flow of cold helium entering the loops the walls can be cooled down, especially those in the steam generator with 60600 kg of iron mass per loop. The effect can be shown by the temperature of the lower reactor plenum which drops significantly. If the helium mass flows were smaller, the energy stored in the walls would be high enough to heat up to near-design values the helium for several minutes.

The result of this severe subcooling is that all nominal temperatures shown are below 700 K at the time of flow reversal. The frequency gradient of the circulator is so great that when reaching standstill the helium masses in the plena next to the circulator do not have time enough to be transported in order to produce a new pressure profile at zero flow.

Fig.3.3 shows the mass flows through the core. During forced convection the distribution of mass flows to each of the links is nearly invariant.

The mass flows first reverse in both outer rows of the radial blanket subassemblies, then in the inner row of the radial blanket, and then in the core beginning in the core center gradually moving to the core periphery. Fig.3.4 shows the axial helium temperature distribution in the core center subassembly (link 7) and the radial blanket (links 17, 18, 19) just before flow reversal occurs. The core center is already heated up again (see fig.3.2), the temperature gradients are so great that the lower axial blanket with its high heat capacity suffers from a delay in temperature rise relative to the rest of the pin, so that the helium is cooled in that section. The temperatures in the radial blanket have reached the minimum, the cooling period of the helium temperatures just being finished. To demonstrate the effect of relative heat generation in the fuel, fig.3.4 shows also the ratio of the actual linear rating to the helium mass flow per pin which, in the PHAETON2-model, is uniform along the axial distance of a node. For convenience, the step increases at the boundaries of the nodes have been delimated by straight slopes. It shows that the axial blanket heat generation is relatively low for link 7 (core center). Therefore, the helium temperatures in this link start to rise effectively only outside the blanket region, the effect being intensified by the delay in temperature rise like in the lower axial blanket. In the radial blanket the delay effect points in the other direction because we are just at the end of a cooling-down

period. Moreover, the heat generation in the lower and upper ends of the pin is relatively high because the fuel consists of the same fertile material all over the pin.
The helium temperatures in link 18 are higher than in all other links, so that the gravity forces acting against the driving pressure differences are minimum and flow reversal occurs first in this link. Link 17 is relatively cool because the relative flow resistance is smaller than in links 18 and 19. The design mass flow of link 17 has to be greater with the higher level of heat generation.

At the design point the flow of link 17 has not yet reached laminar conditions, and during the transient the flow resistance drops with the square of the mass flow. Links 18 and 19 approach laminar condition already at the design point, and their flow resistances drop but proportional to the mass flow. Consequently, for shut-down conditions, the mass flow through link 17 is relatively high because of the relatively low friction forces.

Questions arise whether under low-flow conditions, the velocity profile in the blanket subassemblies is distorted by natural convection effects. Although at time = 3oo s a quasi-steady temperature distribution has not yet been reached a first assessment can be made. For link 17, 18, and 19, respectively, the Reynolds numbers are about 28o, 5o, and 4o. At time = 3oo s, most of the blanket cladding must be heated by the entering fluid flow, so the average film temperature differences are very low. It has been assumed that the film temperature differences have already reached quasi-steady values, which would be approximately 2oK, 5K, and 2K, respectively. With these data the Grashoff numbers are about 13oo, 21o, and 13o. For low Reynolds numbers /5/ has shown that the velocity and temperature fields are unique functions of Grashoff divided by Reynolds, the values of which are given by 4.6, 4.2, and 3.3, but for these small values a distortion of the profiles is negligible. The main reason for this is that, locally, not much heat is transferred to the fluid in the radial blanket, whereas the driving natural convection head, which is produced by the energy transport from the core to the heat exchanger and the

resulting density distribution, imposes a flow rate onto the flow channels which, considering a radial blanket pin, has the character of forced convection. During flow reversal, Reynolds numbers might come out to be so small that the critical Grashoff to Reynolds number, which is greater than 10, might be reached. It has been shown that in the radial blanket heat capacities cause very slow temperature transients so that partial recirculations are negligible as long as they do not occur during intervals longer than 10 seconds.

In the inner row of the radial blanket subassemblies (link 17) the high radial power skew is neglected because the one-dimensional calculations take into account an average pin only. With helium flowing downward through the subassembly, this leads to substantially higher fluid outlet temperatures /6/. Here, critical temperatures might only occur after the flow reversal so that increased local effects of natural convection lead to higher velocities on the hot side of the subassembly. Unfortunately, for the presumed power ratio of 1.5 of maximum to average subassembly power (which is near that of the steady-state design value), the temperature rise is reduced by less than 5%, if we use gross hand calculations valid for time=300s. Realistic values can only be achieved if at least two-dimensional calculations are performed taking into account cross mixing and distortions by spacers or wire wraps. On the other hand, a quasi-steady temperature profile has not been reached at time=300s, and heat capacity phenomena are still more important. Since the level of shut-down heat production is very low, the history of the helium temperatures is in a predominant way a function of the heat capacities and the mass flows. Therefore, link 17 is cooled down more effectively. Once initiated in the core, the flow reversal is pushed forward by the pressure difference across the circulator. This leads instantaneously to high negative mass flows. Consequently, high rates of energy are transported from the core to the upper plenum the temperature of which starts to rise almost without delay. So, the temperatures in the upflow leg can be increased to support natural convection

in the whole loop. While constituting a new temperature profile, which is extremely different from that at the design point, the heat capacities, mainly of the structural material, play a major role. Fig.3.5 shows the axial distribution of helium and clad temperatures in links 7 and 17 at three different times. In the core region, the left-hand side of the cladding surface is smooth while the right-hand side is roughened, leading to an increase of the heat transfer coefficient and a decrease of the driving temperature difference. It is obvious that the temperatures are decreasing during the first two minutes and that the axial temperature gradient has to be reversed after flow reversal. Because of the relatively high heat capacity adjacent to a low mass flow in the radial blanket (link 17), the temperature profile reverses but slowly.

The same phenomena can be shown in fig.3.6 where the radial temperature distributions of the center node of links 7 and 17 are plotted. The gap between the pellet and cladding has been increased from nominal zero to 1 mm for better graphical representation. The temperature variation in helium is fictitious, the mixed medium temperature at the right-hand side being the calculated value. The temperature profiles of the core vary much more quickly than those of the radial blanket. Although in the first 7 seconds the temperatures in the core pins are reduced drastically, the radial temperature gradients are greater before shut-down. Consequently, no trouble arises with thermal stresses in the cladding during severe transients apart from the thermal fatigue problem.

In the course of development of natural convection the cladding temperatures in the core rise to a maximum and decrease when the natural convection has been fully stabilised. The value of the negative mass flow is a function of the density difference between the downward and upward legs of the natural convection cycle. Here the main level of temperatures is rather low so that the necessary density difference is reached at a relatively low temperature difference. The temperature difference is about 220K while it needs 330K in

fig.2.2 where the main temperature level is higher and further explanations are given.

Fig.3.7 shows the power due to the momentum acting on the impeller and the shaft. The frequency of the circulator has been added. As already mentioned, the friction momentum of the shaft is constant, so that the power is proportional to the frequency. The power transferred to the fluid by the impeller is read from the circulator tables; it drops rapidly with decreasing frequency. The power of the shaft becomes bigger than the power of the impeller after time=75s; consequently, the frequency stops to decrease in a near-exponential way. After time=130s the influence of the impeller is so small that the frequency decreases almost in a linear way.

In fig.3.8 the axial temperature distribution in the heat exchanger is plotted for a number of selected instants, where time=180s stands for the situation just before flow reversal and time=190s for the situation just after flow reversal.

The upper graph always represents the helium temperature whereas the lower graph belongs to the temperature of water or steam. For time=0 only those temperatures are registered which are below 650K, showing a long zone of water heating up to the saturation temperature. During transients this zone is reduced considerably. Moreover, the zone of superheating is reduced to zero, leaving almost the whole effective length near the saturation temperature. To avoid that too much wet steam leaves the heat exchanger, the feedwater mass flow would have to be reduced. This would lead to even higher temperature gradients in liquid water. The limited area of this gradient moves away from the feedwater inlet with the time going on; a considerable step can be observed during flow reversal of the helium loop. The complex conditions in the heat exchanger can be seen at the graph for time=300s. Here, the temperatures of the iron structure are plotted as well. The wall inbetween the water and helium faces a temperature near that of water

because of the good heat transfer coefficient on the secondary side. The heat balance is mainly influenced by the energy stored in the walls. The helium temperature is by a minor percentage influenced by the temperature of the peripheric walls of the heat exchanger. Gradually, but very slowly, the distribution of helium temperatures changes from that of a normal counter flow heat exchanger to that of a parallel flow heat exchanger. The entrance conditions of the graph are also strongly affected by the heat capacities of the adjacent tubes. In conclusion, relatively invariant entrance and exit conditions can be observed. They can be strongly distorted if one allows more feed water to enter the heat exchanger so that the exit temperature no longer depends on the saturation temperature. After flow reversal this would be positive, because the temperature of the lower reactor plenum could be decreased, thus leading to a lower temperature all over the helium loop and the reactor core. The high increase of the grid plate temperature, which follows the temperature of the upper reactor plenum with some delay, could thus be decreased effectively.

Comparing figs.2.1 to 2.5 with figs.3.1 to 3.7 we can find some general rules although the input data are not similar.

Core and blanket behave very differently because of their extremely different energy density of the heat source and the resulting characteristic of flow resistance.

The first response of the cladding temperature during a flow-coast-down accident with scram is very sensitive to the inertia of the circulator. For the future history of the accident transients it is favourable to cool down the core cladding while the circulator still has a significant speed. This leads to higher circulator inertias than that of a combined unit with a steam driven turbine. The more effective the cooling period is, the stronger will be the driving forces for natural convection after a fully developed, reversed flow.

Flow reversal occurs first in that link of the core that delivers the smallest gravity force, i.e. the column with the smallest mean helium density. The friction forces at the moment of flow reversal have no decisive influence on which link reverts first.Nevertheless the density profile along the axial distance of a link is a result of the heat capacities and of the history of the heat generation and relative mass flows, and thus it is a function of the friction forces.

Flow reversal occurs first in the reactor core while the temperatures in the adjacent loops are still distributed in such a manner that the upflow leg is cold and parts of the downflow leg are hot. This reduces natural convection forces like in a cold chimney. Two effects are helpful to accelerate the departure from a "cold chimney" status. Firstly, the mass capacities together with a steep run-down of the circulator lead to a fast flow reversal with instantaneously high negative mass flow in the core before the pressure distribution along the circulator has reversed. The drawback is that the circulator stand-still comes relatively early and the shut-down heat production is relatively high. Secondly, if the temperatures of the heat source are high, helium of high energy density is transported to the upper plenum after flow reversal, thus increasing the temperature of the "chimney". The drawback is that high cladding temperatures must be allowed.

As the maxima of the cladding temperatures are the most sensitive values during the transients the first method should be favoured.

Fig.3.9 shows results of two accidents in the 13-link hanging core model combined in one graph. The first accident which is calculated between time=0s and time=240s is that of figs.2.1 to 2.5 (F2-case). The second accident which calculated between time=0s and time=300s is that of figs.3.1 to 3.8 (F3-case). The uppermost part shows on a linear scale the temperatures of the upper and lower reactor plena. The differences of the

histories of both accidents can clearly be seen, the main statement being that the driving temperature difference for natural convection must be higher for a higher temperature level. The lower plenum temperatures are plotted to show the influences on the pressures which can be seen later on.

The lower part of fig.3.9 is constructed in a semi-logarithmic way. In order to show negative values as well, the ordinate is reflected on the abscissa. For each of the accidents 4 graphs are plotted, one showing the frequency of the circulator which stops at zero, one for the pressure difference across the core (the value is positive, if the pressure in the upper plenum is higher than in the lower plenum), one for the pressure difference across the circulator (the value is positive, if the pressure in the outlet plenum is higher than in the inlet plenum), and one for the negative gravity force per unit area of link 17 (innermost radial blanket subassembly).

The frequencies drop as explained before. When they reach 1 Hz, the frequency-dependent tables of circulator characteristics are left, so that the variation of the values below 1 Hz has no more influence on the results. The results show that for the F2-case the 1 Hz-limit is reached with a smaller gradient than for the F3-case. During the cooling-down period of the accident (see the temperatures above) the pressure differences of the core and the circulator run down nearly proportionally. During this period the pressure differences are mainly results of the hydraulic behaviour of the tube network, i.e. the reduced mass flow leads to reduced pressure drops the requirements of which can be met by shifting the helium mass from one plenum to other. As the mass flow rates are reduced drastically at low circulator frequencies, the thermal effect on the plenum pressures is no more negligible. The coincidence of this together with the increase of temperatures in the core and thus in the lower plenum (the helium flow is still downward through the core) leads to a pressure rise in the lower plenum. For the F2-case the temperature rises by 30K, but for the F3-case by 40K. At the same time, the frequency of the F3-case drops much more rapidly so that the pressure compensation by helium

mass flow is reduced more efficiently. As a consequence, the pressure difference across the core reverts, the lower plenum pressure becoming greater than the upper plenum pressure. This phenomen is more effective for the F3-case. If the driving pressure difference drops below the graph of the negative gravity force per unit area of a link concerned, the helium flow reverts in that link. The friction forces are about 10% of the gravity forces shown at the time of flow reversal, which means that they play only a minor role while this effect continues. As all parallel links considered are subject to different gravity forces, the flow reversal is initiated at different instants during the transient. The first response of the network on the flow reversal is that the pressure difference across the circulator stops decreasing before it reaches the zero mark. This is done earlier for the F3-case, thus resulting in a higher driving pressure difference across the circulator. The second response of the network is a thermal response because just after the flow reversal hot helium enters the upper reactor plenum which stops the rapid decrease in the driving pressure difference of the core. For the F3-case this effect comes rather late because during its fast transient (greater temperature increase of the lower plenum combined with rapid decrease of circulator driving momentum) the driving pressure difference of the core grows considerably faster than the forces acting against it. In the remainder of the network, the pressure difference across the circulators helps to increase negative mass flows for the F3-case more effectively than for the F2-case. As negative mass flows are built up, the temperature effects on the pressure distributions are reduced relative to the effect of mass transport. This increases the influence of circulator flow reversal on the acceleration of the helium flow in the core for the F3-case.

All these local effects are part of the overall natural convection capability of the loop. The natural convection is indeed initiated by these local phenomena the history of which is a function of the run-down parameters of the accident. The flow reversal once initiated is globally

backed up by the density differences which are gradually increased by reverting the temperature profiles in the core and afterwards outside the core in the adjacent loops. The time to reach temperature reversal is smaller for the F3-case because the temperatures in the plena before the flow reversal are much closer to each other.
Some general remarks on both cases can be made:

a) The history of the cooling-down period of the accident establishes boundary conditions of significant influence on flow reversal.

b) The reversal of the driving pressure difference across the core is mainly a response to the variation of thermal energy in the adjacent plena.

c) The sequence of flow reversal depends on the actual gravity force of the helium column in the core channel.

d) For the frequency gradients of the design described here flow reversal always precedes a reversal of the pressure difference across the circulator.

e) The behaviour of the circulator helps to initiate flow reversal in the loops.

If, in a downflow core design, natural convection does not immediately follow the run-down of the circulators, the flow reversal may not be started effectively.
A very important feature for this effect is that the longer natural convection is inhibited the longer the period of building up unfavourable temperature profiles may last. Due to the rather low mass flows at the beginning of a natural convection phase the heat capacities dominate the development of any new temperature distribution. Circulators which have a very low frequency gradient at low flow conditions are likely to result in unfavourable condition for initiating natural convection in downflow designs.

## 3.4 Flow coast-down accident in a standing core version with elevated auxiliary heat exchangers

The standing core model of fig. 4.0 is used, the core performing with the "old bundle" and non-elevated steam generators. In fact, the reference design shows that the centre of the heat exchangers is a little bit below the centre of the core. Transients are beginning with a loss of power for all circulators. Scram activities are initiated with a delay of 1.15 s. The feed-water of the secondary loop is proportional to the helium mass flow down to a minimum of 3.7 %. The moment of inertia of the circulator is 6.7 $Js^2$, which is the value for a circulator connected to a one stage steam turbine. It is assumed that for the first 23 minutes enough steam is available to run the circulator at 6 Hz (2.8 % of the design frequency).

In the model an auxiliary loop has been added standing for one of three loops available. The centre of the auxiliary heat exchanger is elevated 10 m above the core thus giving a high natural convection potential. Here, the results for only one auxiliary loop being modelled show some tendencies of the phenomena during the activation of the main-loop isolation valves. If three parallel auxiliary loops are calculated by one model-loop, a perfectly simultaneous behaviour must be presumed. Thus, the present example gives a qualitative view on the circumstances during activation procedure for one loop or three simultaneous loops. For any other history, the results immediately at the critical switch from main loop to auxiliary loops should be substantially different. These versions have not been checked, because of the lack of input data especially concerning the isolation valves. In the present model (see fig. 4.1), the ciculator runs down linear to zero between time = 1400s and time = 1408 s. When the circulator reaches stand-still the main loop isolation valves are closed and the auxiliary loop is opened. The mass flow through the core which is shown in the graph reverts before the circulator stops. It quickly gains zero again after the closure

of the isolation valves. The natural convection in the auxiliary loops starts with a delay, because the upflow leg must be filled with hot gas. Thus, the mass flow through the core stagnates for about 20 s. The temperatures in the core start to increase very rapidly. Because of only one auxiliary loop been modelled, the shut-down heat cannot be removed sufficiently. Even with three simultaneous auxiliary loops, the rapid increase could not be avoided. This indicates the problematic switch from one parallel loop to another when the back-up loop is only run by natural convection.

To ensure that natural convection starts immediately after the auxiliary loop isolation valve has been opened, the temperature distribution in the auxiliary loop should be similar to the pattern expected for steady-state natural convection flow. Having the auxiliary loops run as bypass-loops of the core would be an easy solution. The main circulators would thus pump helium into the core inlet plenum, and from there a small fraction into the auxiliary loops, in which the isolation valves allow a small bypass mass flow. In the auxiliary heat exchanger, the helium should be heated so that the upper leg is always kept at temperatures, which builds up a natural convection potential. When emergency operation starts, the isolation valves must be activated and the auxiliary heat exchanger is fed by cold water instead of by hot water or steam. It is difficult to define the moment, when the valves in the main loops and auxiliary loops must be activated. From fig. 4.1 it can be derived that the pressure in the upper core plenum increases, because the temperature rises, while there is little or no mass flow through the loops. This evidently is a favourable moment to open the auxiliary loop isolation valve, thus initiating immediately the mass flow through the auxiliary loops, since the main circulators running at very low speed act as isolation valves. Obviously, the main loop isolation valves should be closed as well, because the isolation effect

of the circulators is effective over a short period only. In fig. 4.1, these positive responses were not simulated, because of the dominating effect of the anticipated switching sequences.
If the auxiliary loop is run parallel to the main loops with the auxiliary circulators permanently in the normal operational mode, the reaction to a circulator coast-down would simply be the activation of the main loop isolation valves. The moment this would occur would likely be a function of the main circulator frequency. The behaviour of the auxiliary loops would then be similar to that described in chapter 3.5 which indicates optimistic results for a set of parallel loops running with natural convection.

## 3.5 Flow coast-down accident in a standing core version with failing secondary loops

For a standing core with the "old bundle" the model of fig. 5.0 has been established to calculate 2 parallel loops with elevated steam generators. The first model loop represents six helium loops in which during the loss-of-flow accident the heat exchangers perform in a correct manner. The second model loop stands for two helium loops with damaged secondary loops. Here, the feed-water pump of the secondary loops are supposed to fail. Fig. 5.1 and 5.2 show the main output variables of the transient calculations. The accident starts at time = 1s, when all circulators lose power. Normal scram activities are performed by inserting -7$ between time = 2.15 s and time = 2.8 s. The feed water of the secondary loops is run down to a minimum of 3.7 % proportional to the helium flow. The main turbine is bypassed and the exit pressure is reduced to 400 kPa. The friction momentum on all circulator shafts is constant at 590 J which is 5 % of the driving motor momentum at the design point. The inertia of the shaft is 33.4 $Js^2$ which is the five-fold value of a single-stage steam turbine design.

The frequency of the shaft decreases rapidly down to zero where it is supposed to remain for the rest of the time, the circulator acting as a throttle valve only. At time = 15 s the feed-water flow of the two damaged secondary loops stops. The $H_2O$ mass inventory of the steam generator is supposed not to exist from that time on. Per reactor loop this is 6200 kg of $H_2O$, but the mass of the iron tubes of the steam generator sums up to 60600 kg. By neglecting the heat capacity of the remaining $H_2O$ the errors are but small.

Furthermore, the mode of natural convection has already been reached at time = 30 s and helium temperatures are changing but slowly in the damaged loops. This can be seen indirectly by the ratio of nomalized mass flow of the damaged loops to the normalized mass flow of the intact loops. Between time = 15 s and time = 30 s this ratio changes rapidly because the high helium mass flow forces the iron wall adjacent to the helium to change its temperature distribution rapidly because no heat sink on the secondary side exists. With no forced convection remaining, the ratio of normalized mass flows varies in a complex way. The main effect during the first 500 s of the problem is that helium transports energy to the cool iron structure on the downflow end of the damaged loops, thus reducing but slowly the driving temperature difference of natural convection.

Fig. 5.3 shows the history of the temperatures of the reactor inlet and outlet plena, and of the plena of the damaged primary loops, the denominating numbers being specified in fig. 5.0. The first 30 s are dominated by high helium mass flows, the plenum temperatures changing rapidly. Afterwards, the convective energy transport is rather low compared to the energy stored in the iron structure and in the fluid mass of the plena. The time lag of the temperature rise in plenum 7 compared to that

of plenum 2 is about 90 s. Assuming a mass flow of 4.13 kg/s per loop (0.22 % of the design value), the time interval for a fluid particle to run from plenum 2 to plenum 7 is about 10 s. As the fluid volume is much bigger in the heat exchanger, the transport interval sums up to about 240s. Thus, between time = 30 s and time = 200 s, plena 8, 9, and 10 are almost decoupled from plenum 7. The temperature of plenum 8 rises with the fluid temperature at the down flow end of the heat exchanger. The convective time lag between plena 8 and 9 is about 60 s. With these delays and the effect of heat capacity, which will be concidered later-on, the damaged loops behave similar to the intact loops during the first 500 s.

In the model there are two almost vertical and very long tubes of the damaged loop (between plena P2 and P7 and between plena P10 and P1 in fig. 5.0). As the fluid cross section is great the velocities are rather low (2.2 m/s and 1.1 m/s, respectively). It is probable that natural convection effects distort the turbulent velocity profiles. Calculating the Grashoff and Reynolds numbers from the data given by the one-dimensional calculations of PHAETON 2 at fully developed natural convection, which are of course functions of the history of one-dimensional calculations already, we find the Grashoff number to be greater than $2 \times 10^8$ and the Reynolds numbers greater than $1 \times 10^5$. The Reynolds number is fully turbulent. The value for $Gr/Re^2$ is thus 0.02. Below the limit of 0.05 one can assume no gross distortion to exist in the velocity and temperature profiles /7/ of downflow channels. Here, the friction forces will be reduced and the heat transfer will be increased, but not very much. For upflow channels, the flow might be distored over quite large regions and the entrance length of the developing profiles is much greater than for downward flow. When entering a downflow pipe, the flow field becomes very soon stable. During the first 500 s this could lead to a deceleration of the hot gas being cooled

down at the iron structure still at low temperatures in the upflow tube. The acceleration of the energy transport in the downflow tube is less important.

Neglecting these effects the time is calculated which is needed to yield a temperature in the iron structure near the inlet temperature of the damaged loops. The helium temperature in the whole tubing is supposed to be uniform at 1100 K which accelerates the heat transfer to the wall and decreases the balancing time. In the tube P2 - P7 the time to reduce to 1/10 of the original value the helium to wall difference is thus 540 s. The same value is calculated for the tube P10/P1. In the remainder of the damaged links this time would always be longer, and all neglected effects tend to wards the same direction.

With these data known, PHAETON 2 restarts the problem at time = 500 s with the effect that the reduced shut-down heat generation gets balanced, but still with roughly the same temperature distribution in the loops as at time = 200 s. Between time = 505 s and time = 518 s the helium and structure temperature in the links of the damaged loops are raised linearly up to a maximum of $T_{P7}$ = 1090 K (the temperature of plenum P7), thus simulating the heating up of helium during the first 500 s. As a consequence, the plenum temperatures in fig. 5.3 increase as well, but do not reach $T_{P7}$ in the 13 s available, because the entering fluid mixes with the cold helium residual mass in the plenum. After time = 518 s the code restarts normal calculation of the temperatures of the helium and iron structure in the damaged loops by use of the energy balance. The flow reverts because the damaged loops represent a bypass of the core with the intact loops still producing a positive helium flow due to strong natural convection, while the damaged loops lose the natural convection head because of little temperature differences. With the flow reversal, cold

gas enters the damaged loops from the reactor inlet plenum and cools down the iron structure, which rebuilds the capability of natural convection. This effect only occurs in the tube P10/P1 at the end next to the reactor inlet plenum. Because of the tremendous time intervales which are needed to change fluid temperatures in remote areas, the influence of the entrance leg of the flow path is very high. The effective helium column being cooled down slowly, the negative mass flow of the damaged loops is reduced continuously.

Starting with time = 625 s all temperatures in the damaged loops are forced to drop down to 600 K (the temperature of plenum P1) and stay constant for the rest of the time. This procedure simulates the pessimistic history of too much cold helium entering the damaged loops for too long a time. The results show that the bypass is reopened at a certain degree because only little natural convection head is produced with a uniformly low temperature distribution.

Parallel to these results it has been assumed that the temperatures in the damaged loops still increase after time = 518 s. This leads to a uniformly high temperature distribution. The bypass is fully opened by this as no natural convection head is produced, which can be seen in fig. 5.1 (dash-and-dot line). At time = 553 s the change of temperature distribution due to cold helium entering the damaged loops is possible again. The bypass flow decreases significantly and the temperatures in the cladding drop again (see fig. 5.2, dash-and-dot line).

By the whole set of these results it can be shown that the damaged loops tend to isolate themselves and that this effect, even under abnormal condition, is strong enough to prevent maximum cladding temperatures from increasing above the first maximum values at time = 120 s. Because of the big heat capacity

of the iron structure, the second temperature maximum occurs only when the shut-down heat level in the core is below 2.5 %.

## 3.6 Flow coast-down accident during refuelling operation

Natural convection has a high safety potential only at full system pressure. During refuelling, this pressure has to be reduced to 1oo kPa. The reactor has been shut down at least 3 days so that only about 0.4 % of heat has to be removed from the core, and about 0.7 % from the blanket. A frequency of the circulators of 7o % is necessary to keep the temperatures at the refuelling level (core inlet = 36o K, core outlet = 546 K, maximum cladding hot-spot at core center = 591 K, cladding nominal maximum at core center = 557 K, maximum cladding for an average radial blanket pin = 724 K). If the circulators loose power, the density differences in the loop will be too low to cause sufficient natural convection. To increase the densities, fluid mass has to be added as soon as possible. $CO_2$ has a 1o times greater density than helium, and therefore it is believed to be a good substitute in this critical situation. When $CO_2$ is added, it will be mixed with the remainder of helium in the system (132 kg). Assuming that a pressure of 5oo kPa and a temperature of 7oo K are the steady-state variables of the fluid mixture when running on natural convection, one can evaluate the effectiveness of the $CO_2$ fraction. The driving forces of natural convection are proportional to the density, whereas the capability of removing energy from the core is proportional to the product of heat capacity and density.

Fig. 6.1 shows both values as a function of the $CO_2$-mass fraction. The differences between pure helium and pure $CO_2$ are great for the density (factor of 1o) and smaller for the product of density and heat capacity (factor of 2) because of the great specific heat capacity of helium. Both values increase rapidly only for $CO_2$-fractions above 8o %.

Fig 6.2 shows the dynamic viscosity of the gas mixture. The values for pure helium and $CO_2$ are similar; therefore, the variation with the $CO_2$-fraction has only a minor influence on the results.

Fig. 6.3 shows the thermal conductivity, which is by a factor of 1o better for pure helium than for $CO_2$.
The value of the mixture decreases substantially only for $CO_2$-fractions greater than 8o %.
As a result of all three figures one can state that the mass fraction of $CO_2$ has to be predominantly high to assure a high natural convection potential. It is a drawback that the thermal conductivity decreases rapidly at high $CO_2$-fractions.

Adding enough $CO_2$ to 132 kg helium quickly leads to pressures higher than 5oo kPa. Detailed results will be obtained from the PHAETON2 results.

For these calculations the reactor represented in fig. 5.o is used with all 8 loops running simultaneously.
Just before the transient starts the reactor releases 13.7 MW (0.445 % in the core, 0.727 % in the blanket).
The total mass flow is 14 kg/s at a circulator frequency of 148 Hz. In the core center, the radial temperature difference between the pin center and cladding surface is less than 1o K. The axial cladding temperature increase is dominated by the helium temperatures with the highest temperature rise in the radial blanket channel (284 K).

At time = O the circulator speed and thus the mass flow drop to zero within one minute. Fig. 6.4 shows the total mass flow through the core. In fig. 6.5 the temperatures of the core cladding rise almost linear with a gradient of 0.7 K/s if there is no mass flow through the core. After two minutes, $CO_2$ of 5oo kPa and 3oo K is fed for one minute to the reactor inlet plenum. Calculations have shown that this is not sufficient. Thus, starting with time = 28o s, $CO_2$ of 1ooo kPa is fed for another minute. Then, natural convection is allowed to establish. After 2o minutes the mass flow reaches a value which stops the temperature increase and subsequently cools down the core again. The thermal response to the $CO_2$-ingress is dominated by the heat capacities. In Fig. 6.5 the outlet plenum temperature is a main indicator for the natural convection potential. When $CO_2$ is added, its temperature rises quickly, because of the effective removal of thermal energy from the core and because of energy due to compression.
After this first response to forced convection resulting from the type of $CO_2$ inlet parameters, it takes a rather long time to heat up the outlet plenum because of the small mass flows facing big internal heat capacities. The curve of the outlet plenum temperature has thus a delay of about 1o minutes compared to that of the nominal cladding maximum temperature.

Since the internal structures of the rest of the loop are cooled down effectively before the accident, the natural convection is blocked for a long time. Thus, the time lags play a major role in the calculation of the resulting temperature maxima. When all the $CO_2$ is fed to the system, the mass fraction of almost 99 % $CO_2$ is reached. The plugs of the PCRV, which have to be activated during refuelling have to withstand an internal pressure of 1ooo kPa in this position. To add $CO_2$, instead of another high-density, high-capacity liquid during this hypothetical accident has the advantage that only long-time corrosion affects the integrity of the core and primary loops. The results shown in fig. 6.5 gives another evidence for the fact that it is difficult to start natural convection from unfavourable temperature distributions, which has already been seen with the flow coastdown accidents in hanging downflow cores.

In fig. 6.5 the peak cladding temperature, starting from a higher value than that of the core region, increases very slowly. At the end of computer calculations, this value still grows, the rather big delay being a function of the great heat capacity and the small mass flow. A quasi-steady axial temperature rise can be assessed from the values of the blanket power and the product of fluid mass flow and heat capacity at time = 127o s. The value of the mass flow is pessimistic, because the rise of blanket temperatures increases the natural convection potential. But this effect is largely dominated by the small heat capacity of the $CO_2$-He-mixture. Presuming a linear increase of cladding temperatures with time, the point of cladding failure (15oo K) will be reached after 5 hours.

In similar calculations for the accidents shown in chapter 3.2 to 3.5 the blanket cladding temperatures never reached the point of failure. Indeed, they always were less than 13oo K. In these hand calculations the data of the one-link blanket are more conservative than those of the three-link blanket.

## 3.7 Effects of a low pressure drop core on the results

It has been proposed by KWU to design the core such that the pressure drop is reduced drastically. This can be done without major penalty in neutron balance. Simultaneously, it has been stated that a bigger pin diameter would be favourable as well. To compare a new design with the old data, the following parameters have been taken as a basis. The first value stands for the core region, the second for the radial blanket:

pin diameter = 1o mm / 16 mm
pitch of triangular mesh = 15.3 mm / 19 mm
hydraulic diameter = 15.8 mm / 8.98 mm

In the core region one can show that Grashoff and Reynolds numbers can change within a large scale, while natural convection effects are still not able to distort the temperature and velocity profiles of forced convection. This is much more different for the radial blanket, because with the old design data we were already near the border where natural convection distortions cannot be neglected. If we only change the value of the hydraulic diameter in the calculations for the radial blanket (chapter 3.3) the ratio of Grashoff divided by Reynolds will be 18, 16, and 11 for link 17, 18, and 19, respectively.
This should be even an optimistic assessment, because the Reynolds numbers are rather high, when the differences are neglected.
With these numbers, the velocity profile shows a substantial flattening in the center of the channel, and the Nusselt number just starts to be increased. For the innermost radial blanket subassemblies the effect of the power skew upon the flow redistribution inside the cluster increases. No conclusion can be drawn that recirculation could occur in parts of the cluster, because the forced convection influences are still strong.

During flow reversal in the hanging core design, the probability of recirculation within blanket subassemblies for up to 1o s is high. From the results of chapter 3.2, where the net mass flow through one blanket link changed the direction several times, an increase in flow instability could be derived as well. Consequently, the temperature increase of the upper core plenum and adjacent loop volumes would be reduced, and the system would stay at an insufficient natural convection potential for a rather long period.
As already mentioned, a favourable sequence of flow reversal phenomena is strongly influenced by the boundary conditions. If these demands cannot be met, high cladding temperature increases are inevitable.

## 4. Summary

Helium at high pressures is so good a reactor coolant that it is capable of removing the decay heat of a shut down core with natural convection. The design of cores with optimised pressure drop characteristics can readily be achieved. These designs only need an elevation of the heat sink less than 1o m above the core. Compared to carbon-dioxide or sodium coolant, this value is only by a factor of 3 to 5 higher. The inherent features of natural convection can best be shown if, in the designs, valves to be activated are omitted. This leads to the requirement that the heat sinks are redundant and auxiliary heat exchangers are in line with the main evaporators. Running only the primary helium loops by natural convection is not sufficient. Natural convection should be available down to the ultimate heat sink. The secondary auxiliary loops could be designed in such a way that the necessary parameters are obtained.

It can be argued that under these circumstances a standing core design is the easiest way towards a safe design. This design has another attractive feature. Because of the small height of the core as compared to the elevation of the heat sink above the heat source the core is subject to forced convection, which is built up by the pressure differences between the inlet and outlet plena.
Natural convection effects inside the subassemblies are almost negligible and subchannel disturbances do not generally occur as they might do in LMFBRs and HTRs.
This leads to the positive result that the combination of forced and natural convections, or reach of them alone, perform in an inherently stable manner.
There are difficulties in the radial blanket, which could be overcome by a proper design. Subchannel analyses should solve the problem of high radial power variation. This could lead to peak cladding temperatures in the first row of the radial blanket, which are higher than those calculated by the present code. By postponing the efficiency at the design point the subassembly orifices can be adjusted in such a way that the peak cladding temperatures during natural convection, which occur a long time after those in the core, do not reach critical values.

For the amount of energy released under shut-down conditions, the heat capacities outside the reactor are very helpful even if the heat sink fails due to damaged secondary loops. Presuming the capability of subcooling, this leads to very long time constants in the transients of the heating-up phase.

If the natural convection potentials are expressed by $Q/(H \Delta T)$, where Q is the ratio of shut-down heat divided by the full power design value, H is the elevation of the heat sink above the heat source, and $\Delta T$ is the temperature difference between the cold and hot leg of the one-phase fluid loop, an assessment of the values for PWRs and GCFRs leads to a general comparison.
The natural convection potential for water at 16 MPa and 56o K is $2.15 \times 1o^{-3}$ $(m\ K)^{-1}$, and for helium at 12 MPa and about 7oo K it results in $1.23 \times 1o^{-3}$ $(m\ K)^{-1}$.
This should provide evidence that the auxiliary loops can be designed for natural convection, rejecting the energy to a dry cooling tower, which runs on natural convection as well.

Phenomena of forced convection superimposed by natural convection are much more complex for a hanging core (downward flow) than for a standing core (upward flow). The results show that even for the hanging core the cladding temperatures do not reach critical values with the present input parameters. But there is a number of questions, which has to be solved favourably by experimental verification of code calculations. Although natural convection is not as complex in GCFRs as in most other reactors, the transient response to the inserted operation conditions is very difficult to analyse.
The problem of realistically taking into account the heat capacities of the upper plenum and the adjacent tubes cannot simply be resolved by setting the effective tube walls to be 1o mm thick everywhere, as the code does in the present version. It should be noted that helium enters the hugh upper plenum, where complicated mixing phenomena take place. The gas comes into contact with the internal structures and walls, which have complex geometries.

The natural convection makes available the heat capacity of the whole internal structure of all the loops, which increases by a factor of about 4 the overall heat capacity with respect to that of the core. If one takes into account the evaporation enthalpy of the water in the heat exchangers the heat capacity will be increased drastically. With these data, the GCFR is no longer a reactor with an extremely low heat capacity.

## 5. References

/1/ D. Wilhelm, Transient analyses of a 1ooo-MW gas-cooled fast reactor, Nuclear Technology, Vol. 39 (June 1978) pp 3o-4o

/2/ D. Wilhelm, The PHAETON2 computer code for analysing accidents in a 1ooo MWe helium cooled fast reactor, KFK2561, Dec. 1977

/3/ M. Dalle Donne, M. Hudina, M. Huggenberger, L. Meyer, K. Rehme, EIR, KFK joint heat transfer experiments on a single rod, roughened with trapezoidal rounded ribs and cooled by various gases, KFK2675, Nov. 1978

/4/ W. Jung, W. Krug
Gas-cooled fast breeder reactor fuel bundle irradiations in the BR2 helium loops, Nuclear Engineering and Design, Vol. 4o (1977) No. 1, pp 157-17o

/5/ T.J. Hanratly, E.M. Rosen, R.L. Kabel
Effect of heat transfer on flow field at low Reynolds numbers in vertical tubes, Industrial and Engineering Chemistry, Vol. 5o (1958) No. 5, pp 815-82o

/6/ C.B. Baxi
Effect of buoyancy force on the velocity and temperature distribution in the GCFR radial blanket CONF-7711o9--87, San Francisco, Nov. 1977

/7/ J.P. Easby
The effect of buoyancy on flow and heat transfer for a gas passing down a vertical pipe at low turbulent Reynolds numbers, Int. J. Heat Mass Transfer Vol. 21 (June 1978) pp 791-8o1

/8/ "1ooo MWe-Gasgekühlter Schneller Brüter, Referenz und Sicherheitsstudie", unpublished report 1974

| Geometry | old bundle | new bundle |
|---|---|---|
| diameter of the pin | 8.2 mm/13.1 mm | 8.25 mm/13.1mm |
| pitch to diameter | 1.341/1.05 | 1.405/1.11 |
| hydraulic diameter | 7.8 mm/3.4 mm | 9.7 mm/5.4 mm |
| height of the roughness | 0.1 mm | 0.1 mm |
| width of the roughness | 0.1 mm | 0.35 mm |
| pitch of the roughness | 0.7 mm | 1.2 mm |
| fluid cross section area, whole core | 4.25 $m^2$ | 5.66 $m^2$ |
| design point | | |
| $R(h^+)$ | 5.0 | 6.5 |
| Nusselt number, center core, rough surface | 622 | 536 |
| Stanton multiplier of roughness | 2.52 | 1.88 |
| friction multiplier of roughness | 4.97 | 4.49 |
| pressure drop, core | 469 kPa | 300 kPa |
| pressure drop, loop | 112 kPa | 103 kPa |
| total mass flow, core | 1868 kg/s | 2134 kg/s |
| temperature rise, core | 280 K | 250 K |
| core inlet temperature | 544 K | 544 K |
| circulator inlet temperature | 537 K | 537 K |
| power of the motor driving the circulator | 124 MW | 98 MW |
| cladding temperature of core center, nominal maximum | 974 K | 961 K |
| maximal temperature gradient in the cladding of the core center | 102 K/mm | 100 K/mm |
| 3% mass flow | | |
| mass flow per unit area, whole core | 13.2 kg/($m^2$s) | 11.3 kg/($m^2$s) |
| Nusselt number of the fully develloped laminar flow | 9.5/2.7 | 10.2/5.3 |
| Stanton number of the laminar flow multiplied by the Reynolds number | 14.24/4.05 | 15.29/7.95 |
| Fanning friction factor of the laminar flow multiplied by the Reynolds number | 27.6/15.8 | 28.9/20.3 |
| Reynolds number (for core sub-assembly with above whole core mass flow) | 2980 | 3210 |
| Stanton number (for core sub-assembly with above whole core mass flow) | 0.00478 | 0.00475 |
| Fanning friction factor (for core sub-assembly with above whole core mass flow) | 0.00926 | 0.00899 |

second value for radial blanket

Fig. 1.o Comparison between the two bundle designs in use

| link | 7 | 8 | 9 | 10 | 11 | 12 | 13 | 14 | 15 | 16 | 17 | 18 | 19 |
|---|---|---|---|---|---|---|---|---|---|---|---|---|---|
| enrichment zone | 1 | | | | | 2 | | 3 | | 4 | radial blanket | | |
| drag coefficient | 3.30 | 3.38 | 3.41 | 3.79 | 4.03 | 3.42 | 5.25 | 3.43 | 10.66 | 5.06 | 702 | 10002 | 13002 |
| fluid cross section ($m^2$) | 0.018 | 0.108 | 0.216 | 0.216 | 0.307 | 0.523 | 0.307 | 0.631 | 0.416 | 0.956 | 0.600 | 0.652 | 0.714 |
| mass flow per unit area ($kg/(m^2s)$) | 572 | 570 | 569 | 565 | 562 | 571 | 546 | 573 | 487 | 554 | 93 | 22 | 20 |
| Weisbach friction factor in the smooth part $X10^2$ | 1.704 | | 1.705 | | 1.709 | | 1.719 | | 1.760 | | 3.058 | 4.463 | 4.520 |
| subassembly outlet temperature (K) | 807 | 806 | 804 | 801 | 797 | 798 | 795 | 790 | 791 | 772 | 790 | 760 | 727 |

Fig. 1.1 Design data of the "new bundle"

Design point characteristics

| | |
|---|---|
| maximum linear power in the core centre | 42.9 kW/m |
| axial form factor | 1.25 |
| radial form factor | 1.09 |
| thermal power of the core and the blanket | 2779 MW |
| thermal power of the core | 2644 MW |
| power of all helium circulators | 148 MW |
| helium inventory | 10156 kg |
| total steam flow through the heat exchangers | 1088 kg/sec |
| feedwater pressure | 209 bar |
| feedwater temperature | 443 K |
| hot spot factor of the helium temperature difference | 1.17 |
| hot spot factor of the heat transfer fluid-wall | 1.39 |
| hot spot factor of the heat generation in the pellet | 1.17 |

Constant properties

| | |
|---|---|
| specific heat capacity of helium | 5.22 kJ/(kg K) |
| ratio of specific heat of helium | 1.667 |
| Prandtl number of helium | 0.667 |
| gas constant of helium | 2.078 kJ/(kg K) |
| density of the pellets | 9113.4 kg/$m^3$ |
| density of steel (cladding, subassembly wall) | 8000 kg/$m^3$ |
| thermal conductivity of the pellets | $1.9 \times 10^{-2}$ kW/(m K) |
| thermal conductivity of steel | $2.284 \times 10^{-2}$ kW/(m K) |
| specific heat capacity of the pellets | .3349 kJ/(kg K) |
| specific heat capacity of steel | .5862 kJ/(kg K) |

Reactivity values

| | |
|---|---|
| reactivity constant of axial expansion | $K_A = -2.27 \times 10^{-6}$ |
| reactivity constant of radial expansion | $K_R = -7.47 \times 10^{-6}$ |
| reactivity constant of helium density variation | $K_V = -4.471 \times 10^{-3}$ |
| Doppler reactivity | $\frac{1}{k}\frac{\partial k}{\partial T} = .082\ T^{-3/2} - .008\ T^{-1}$ |
| weighting factors for the Doppler feedback: | |
| inner core region | .4939 |
| outer core region | .2250 |
| total blanket | .2811 |

**Fig. 1.2 Major input data for PHAETON 2**

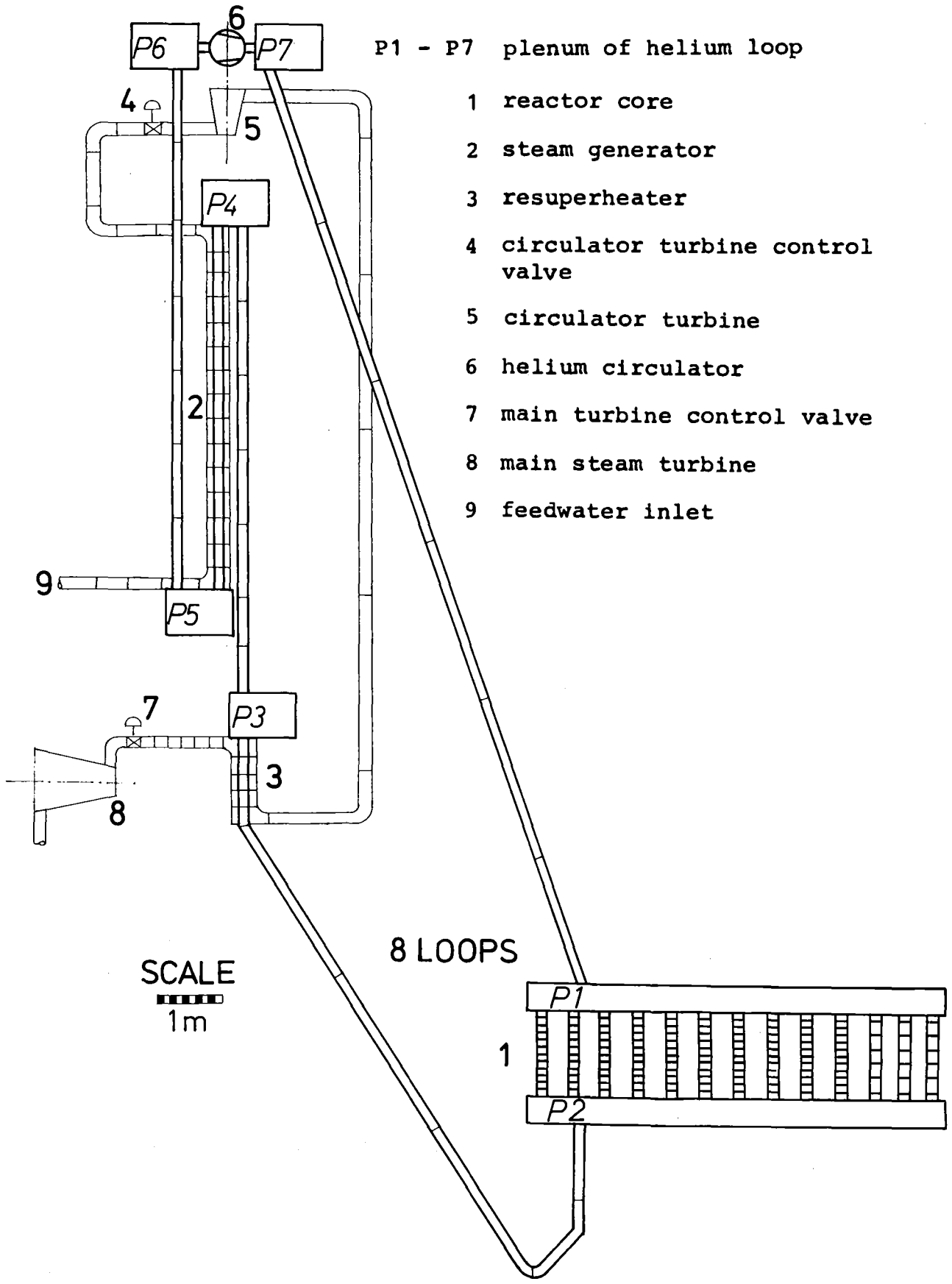


Fig. 2.0 PHAETON 2 model of the 1000 MW reactor with hanging core, 13 core links, elevated steam generators, and steam driven circulators

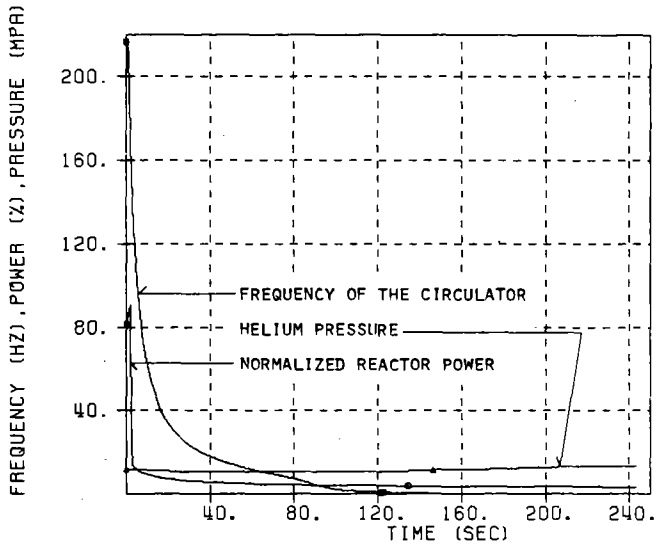


Fig. 2.1

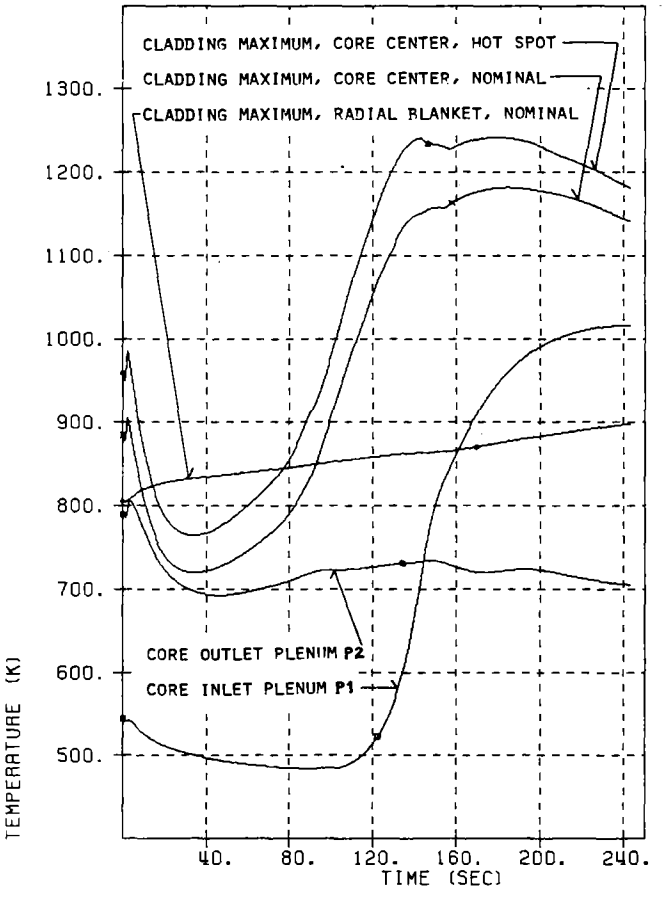


Fig. 2.2

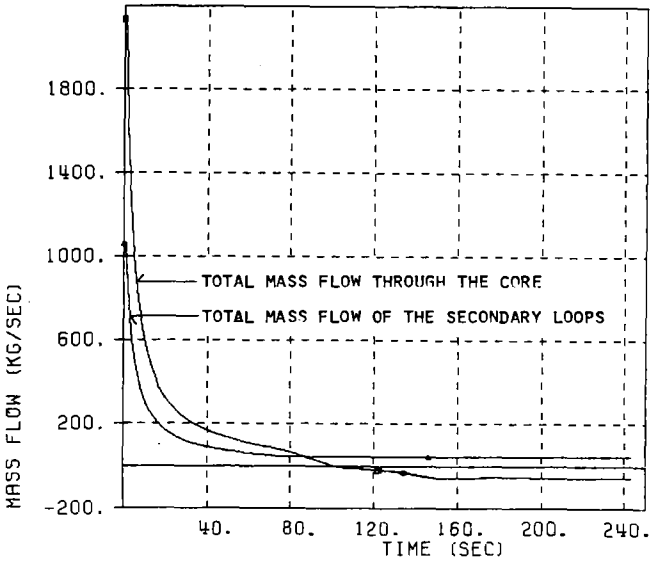


Fig. 2.3

Flow coast-down accident for the model of fig. 2.0

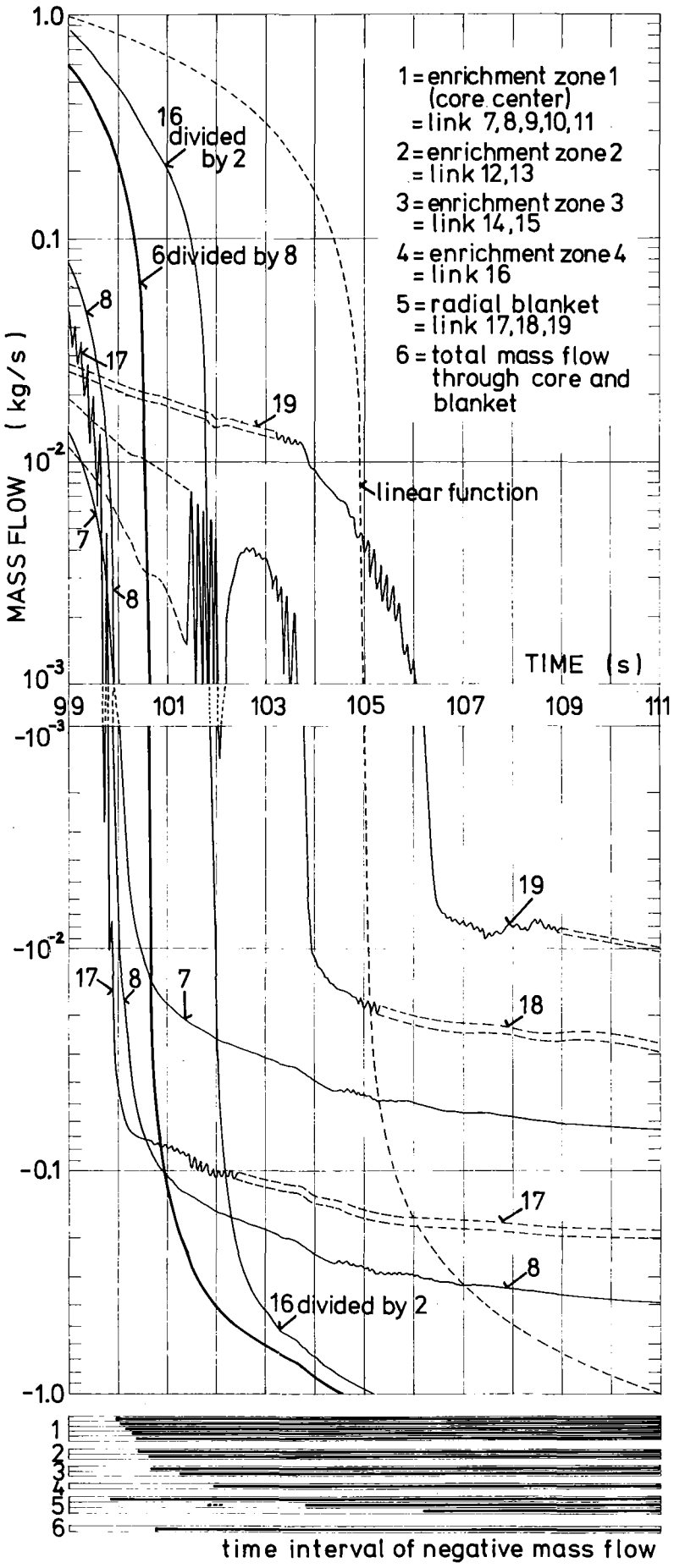


Fig. 2.4 Time interval between 99 s and 111 s of the flow coast-down accident for the model of fig. 2.0

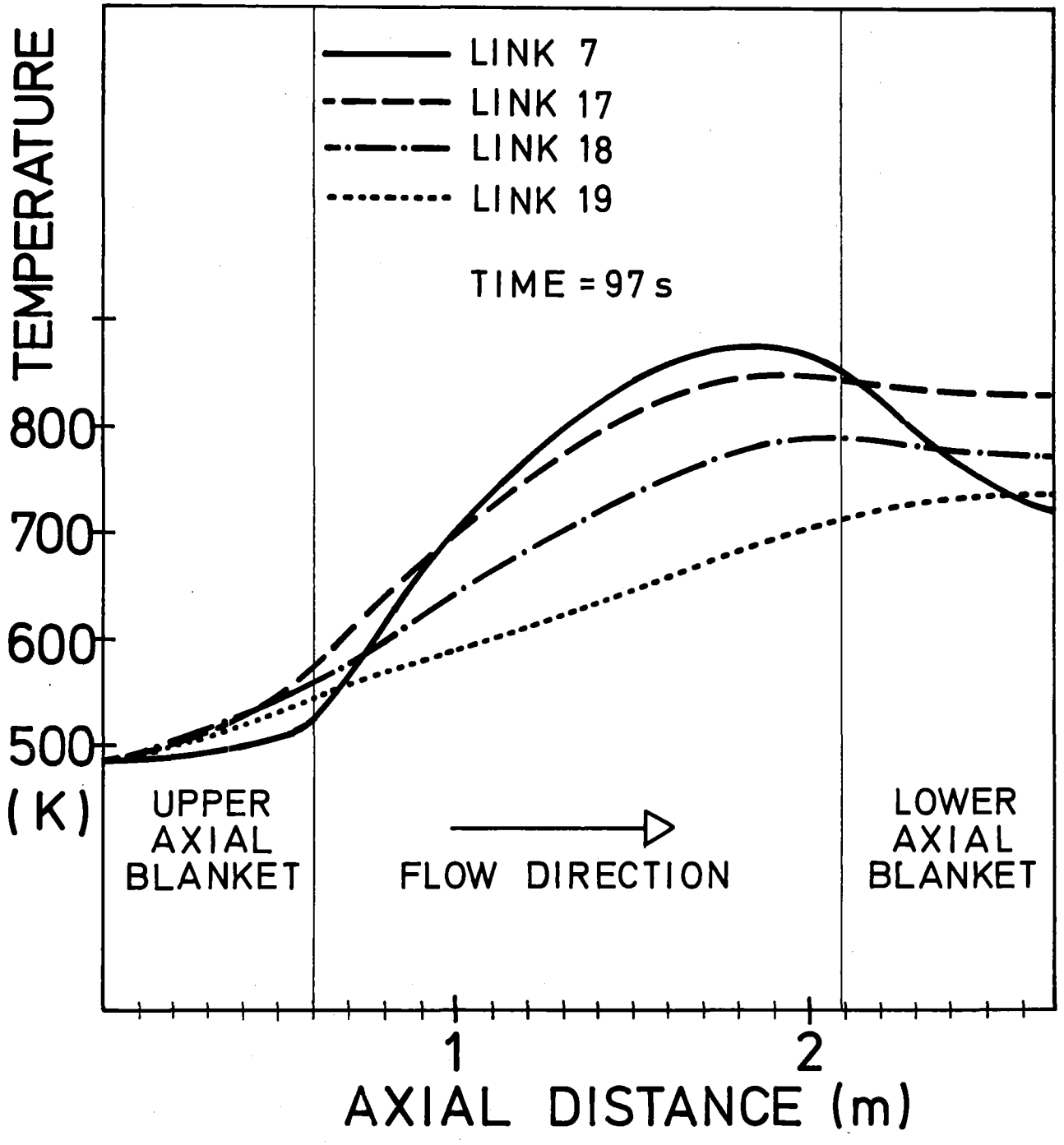


Fig. 2.5 Axial helium temperature distribution shortly before flow reversal

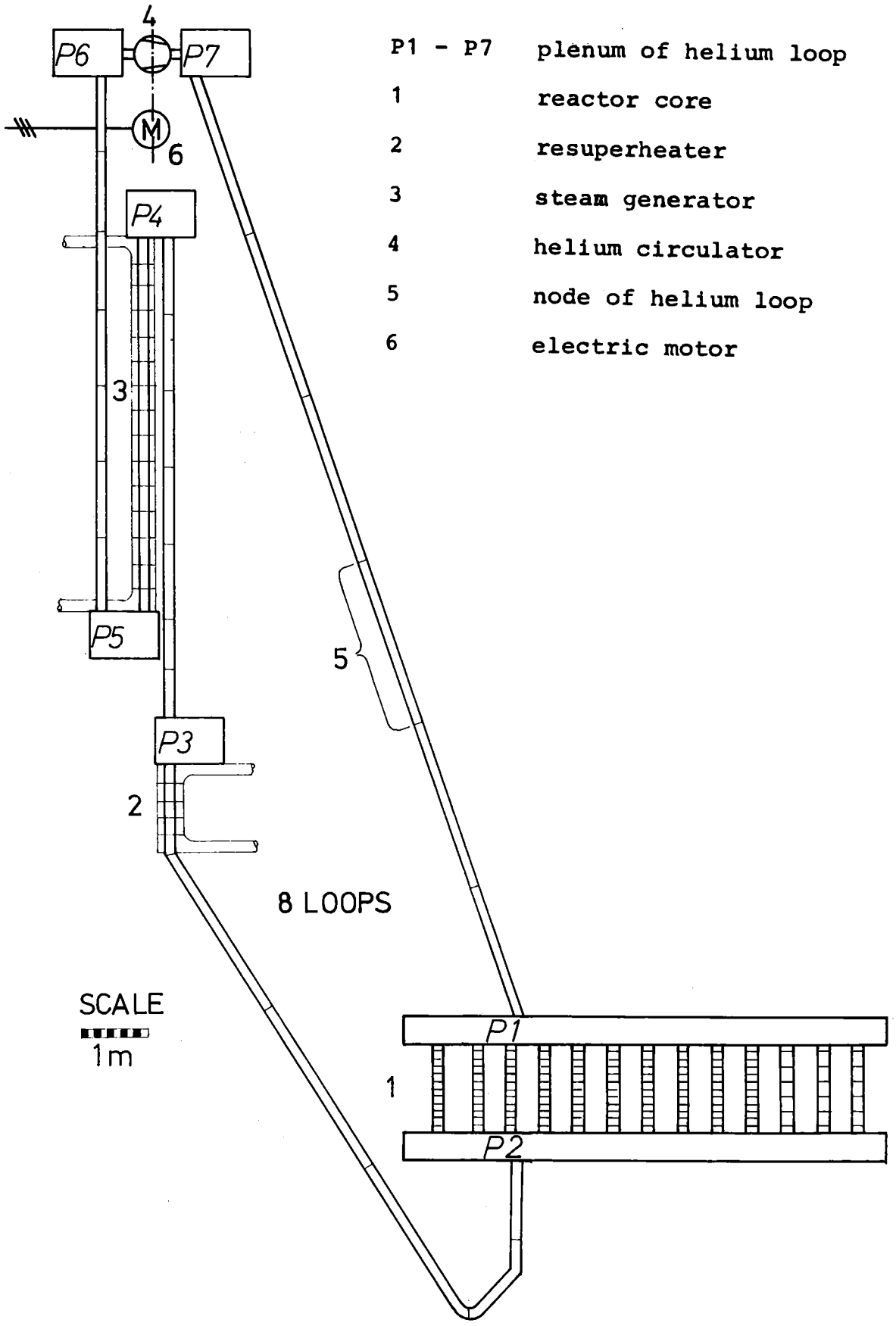


Fig. 3.0 PHAETON 2 model of the 1000 MW reactor with hanging core, 13 core links, elevated steam generators, and electric driven circulators

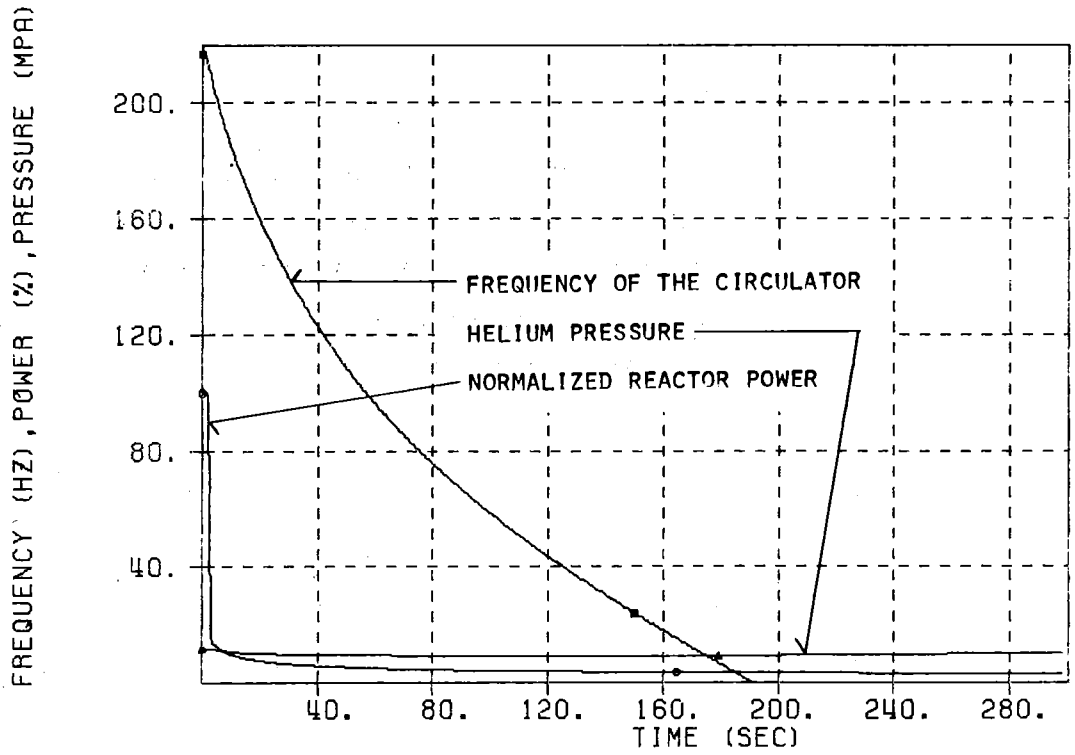


**Fig. 3.1** **Flow coast-down accident for the model of fig. 3.0**

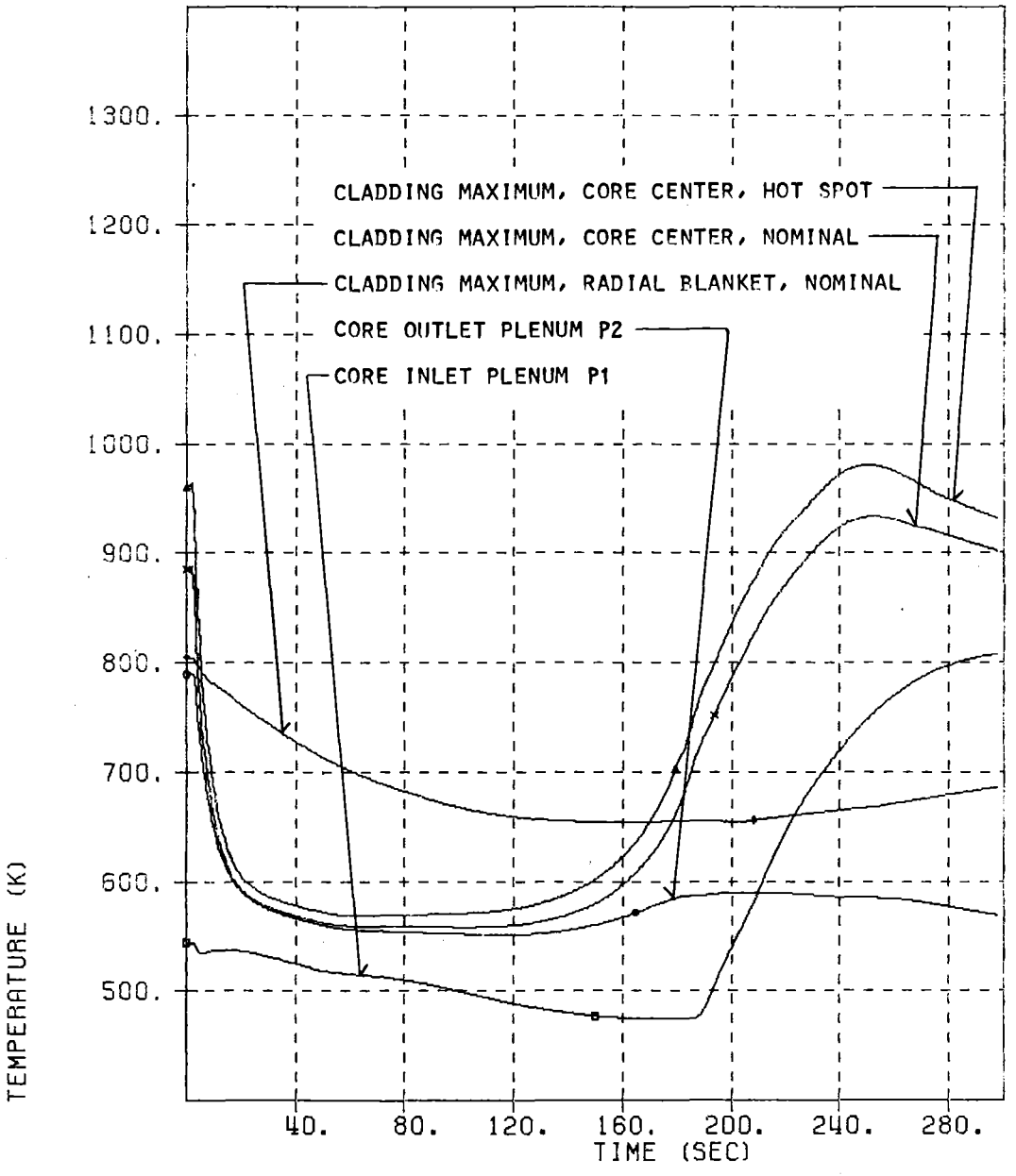


**Fig. 3.2** **Flow coast-down accident for the model of fig. 3.0**

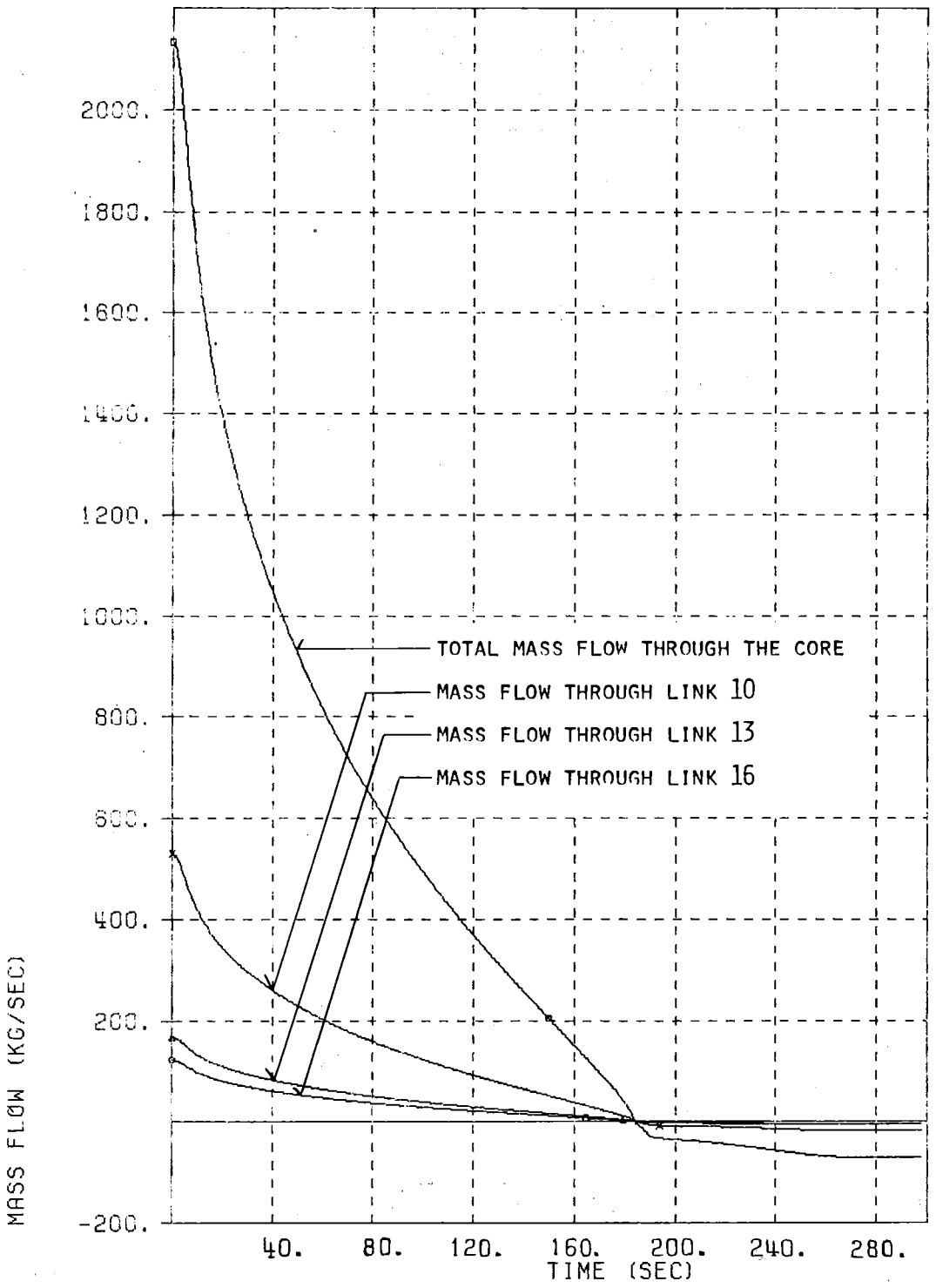


Fig. 3.3 Flow coast-down accident for the model of fig. 3.0

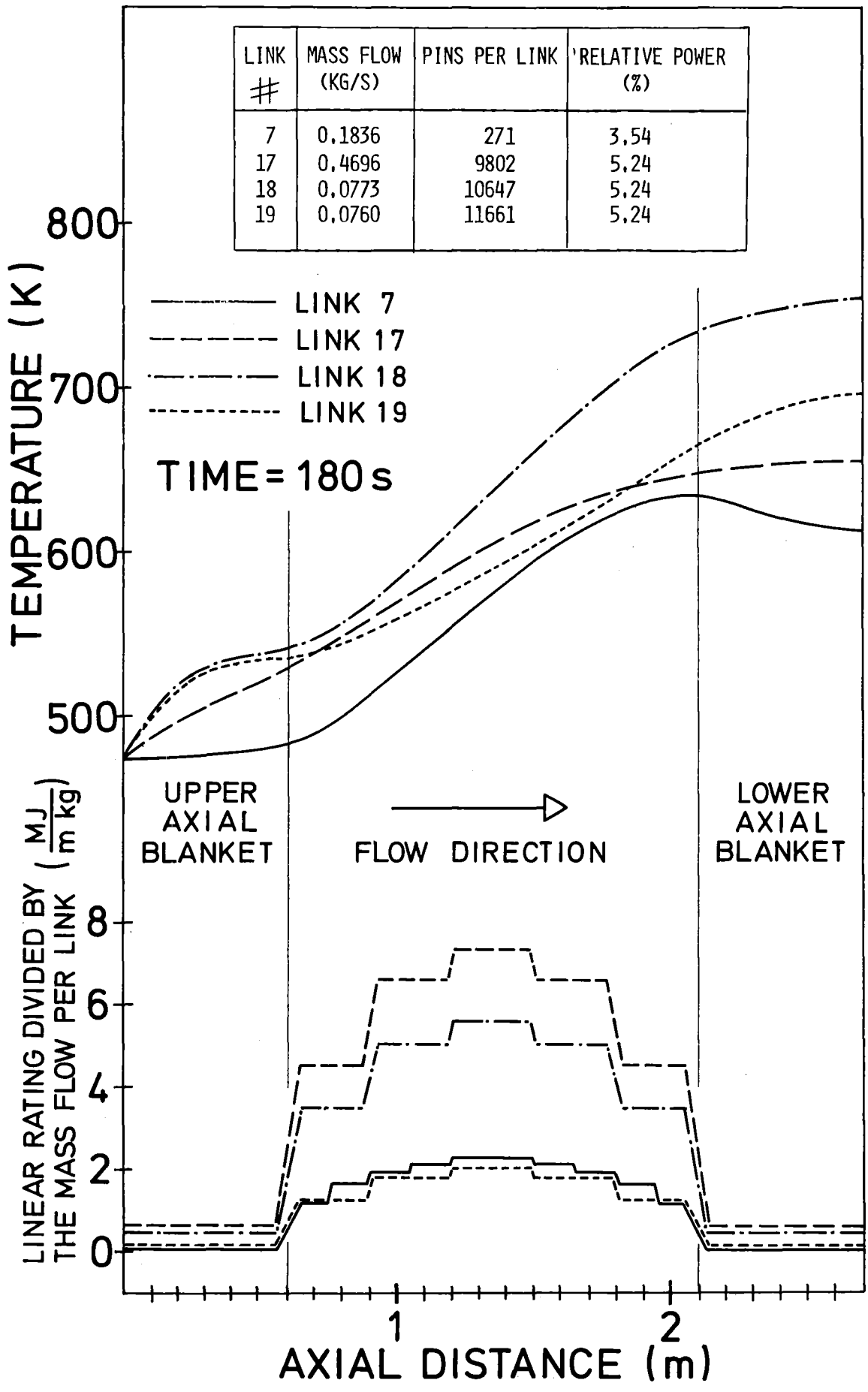


Fig. 3.4 Axial helium temperature and linear rating distribution shortly before flow reversal

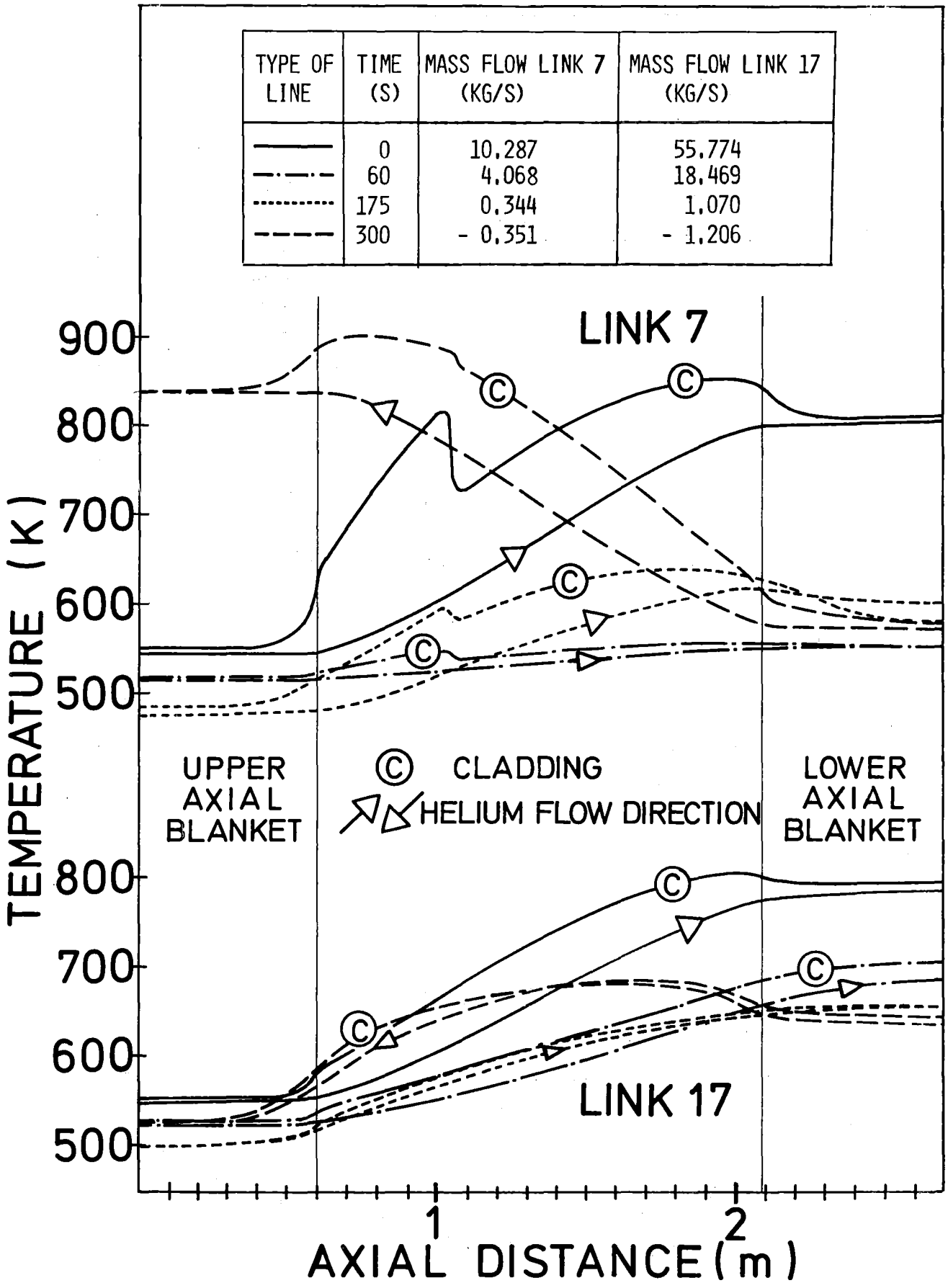


Fig. 3.5 Axial helium temperature distribution at special times

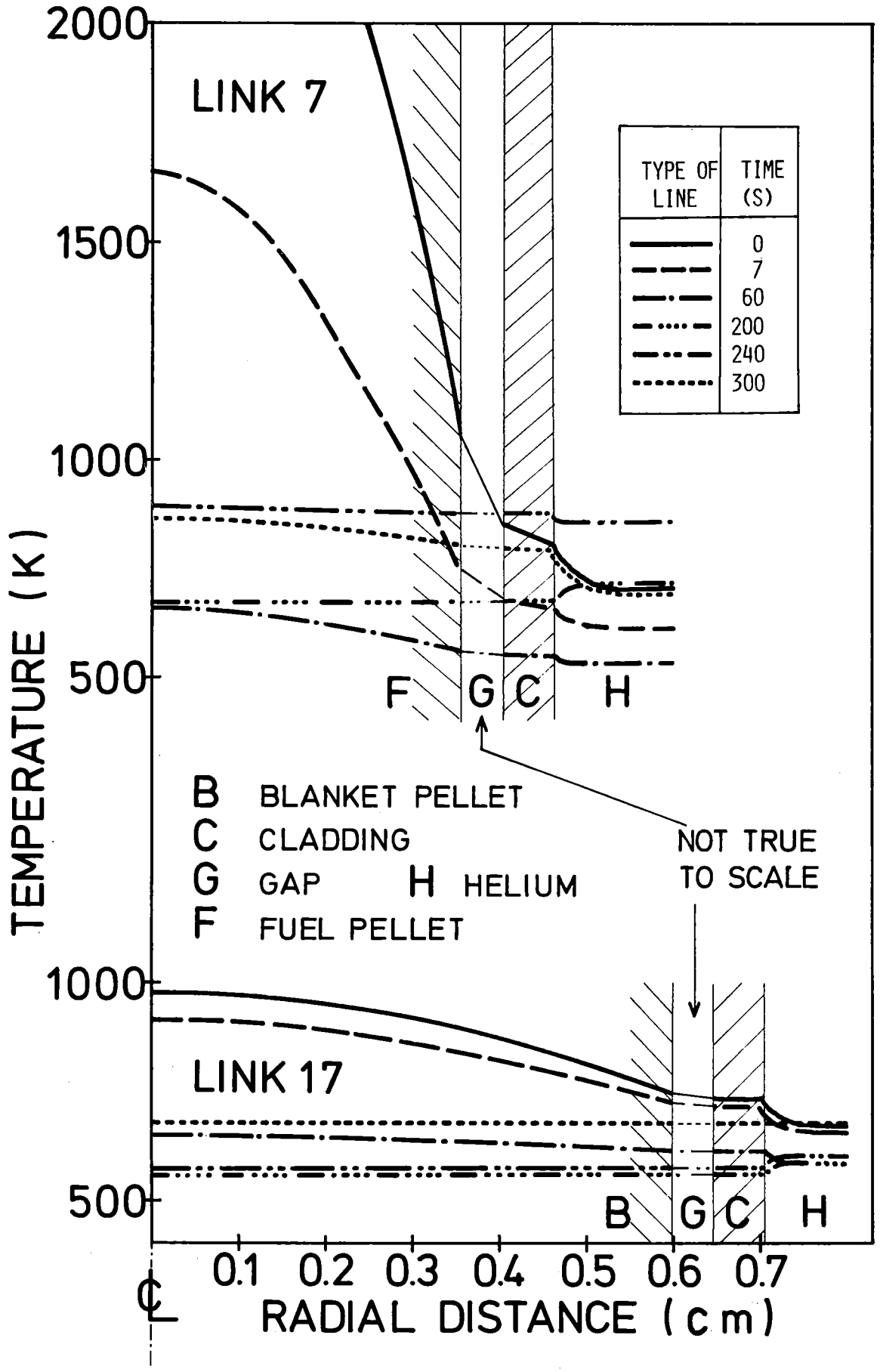


Fig. 3.6 Radial temperature distribution in pins at specified times

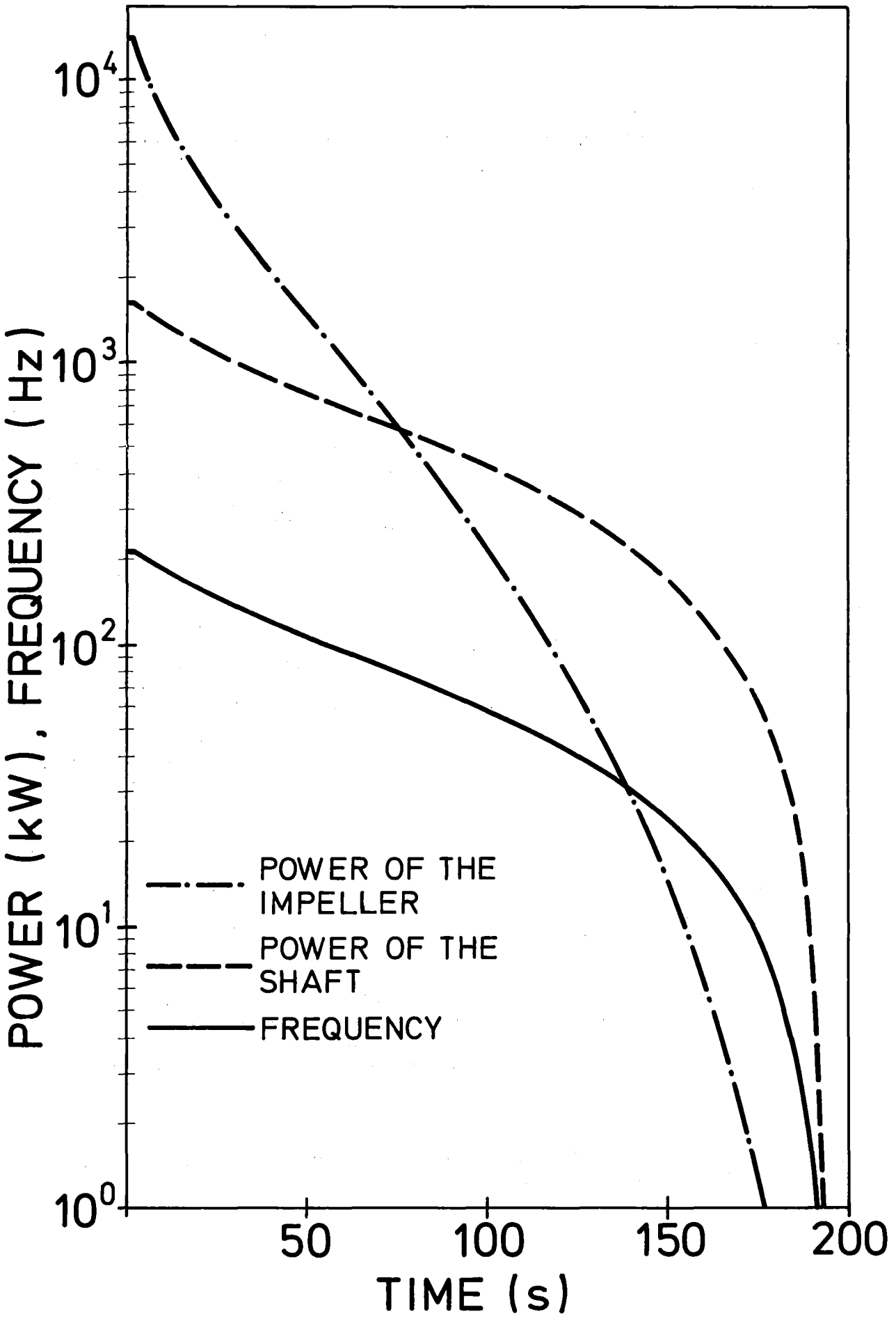


Fig. 3.7 Frequency and power of the circulator

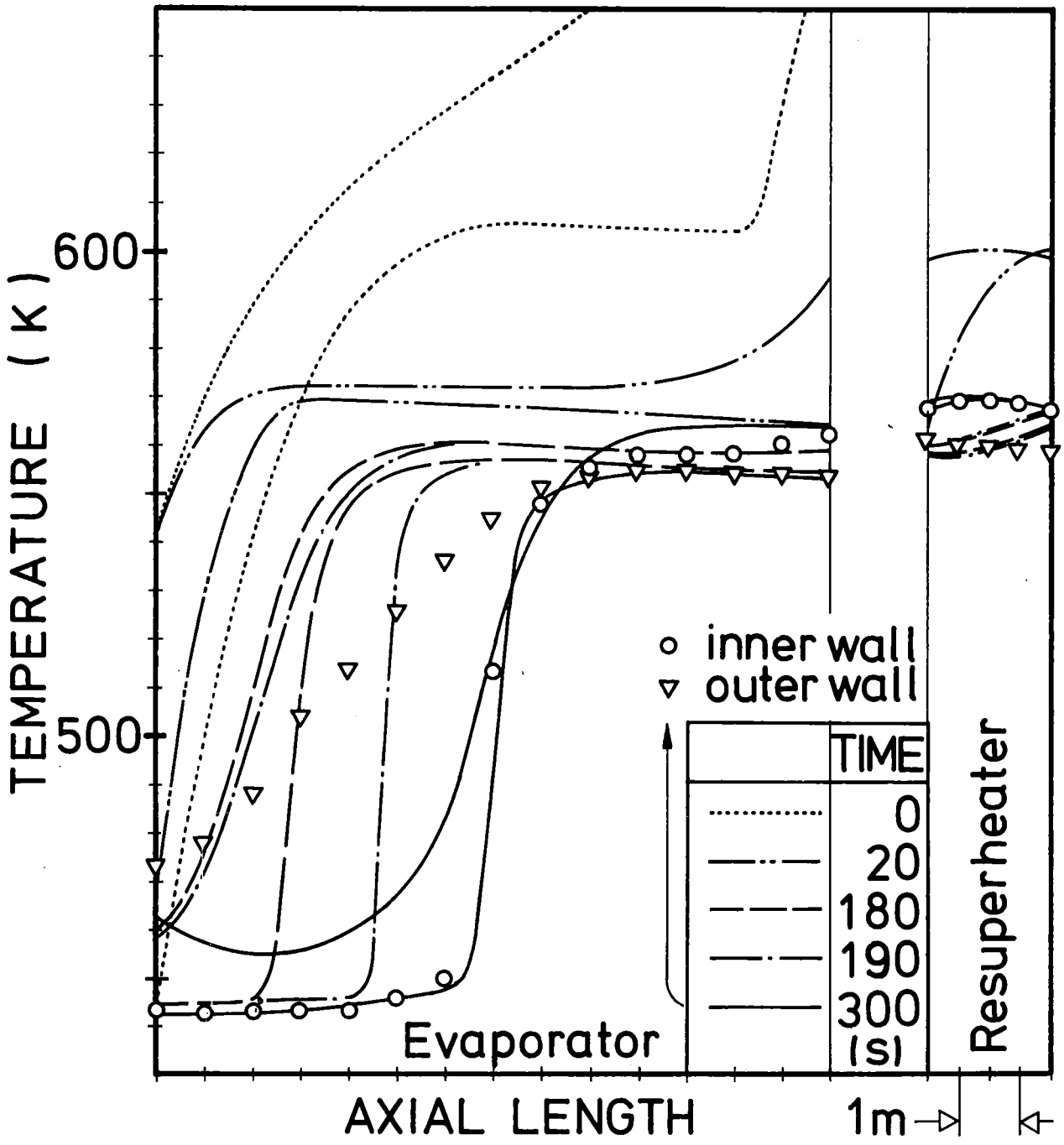


Fig. 3.8 Axial helium temperature distribution in the steam generator at specified times

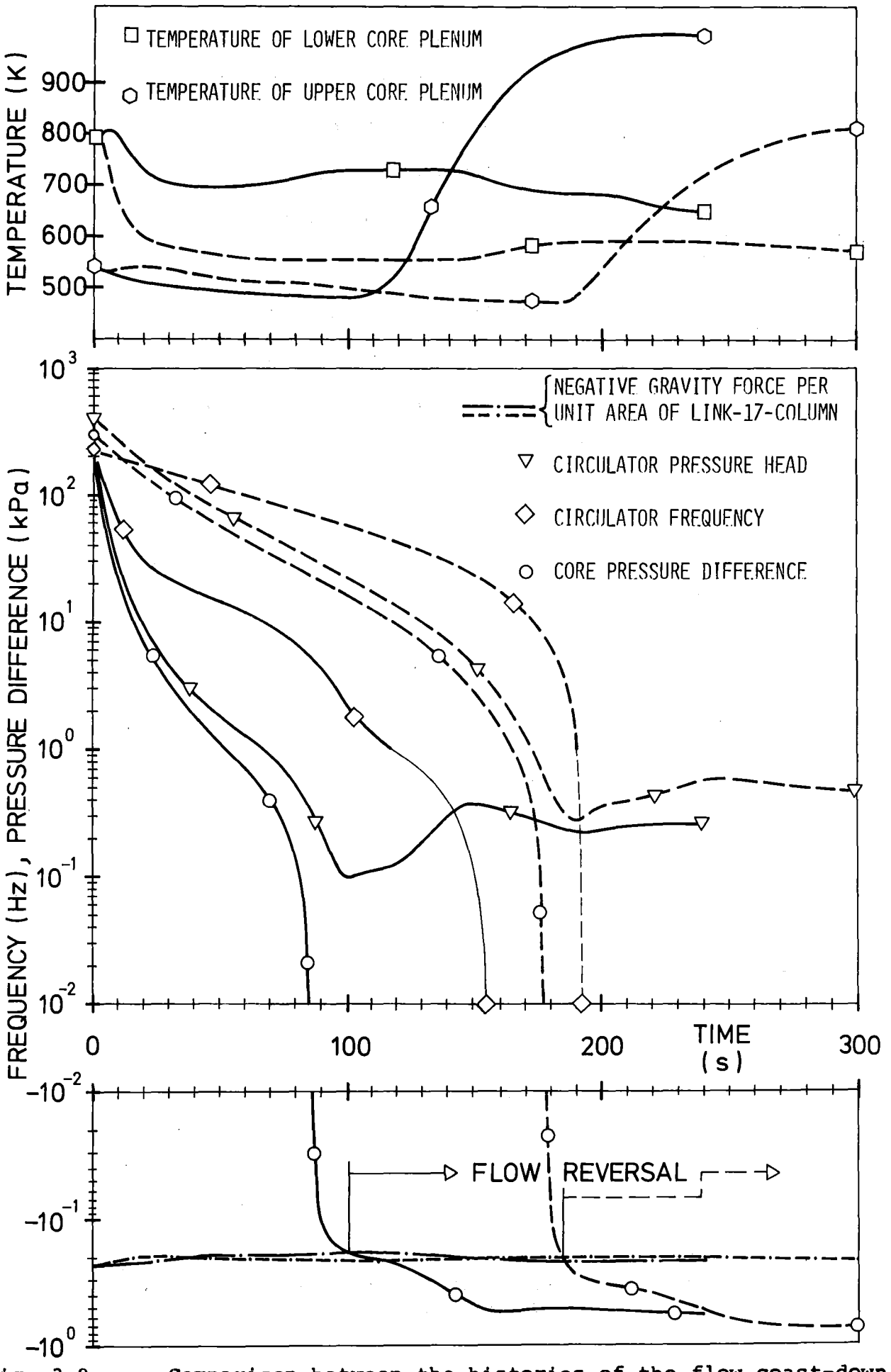


Fig. 3.9 Comparison between the histories of the flow coast-down accidents in the models of fig. 2.0 and 3.0

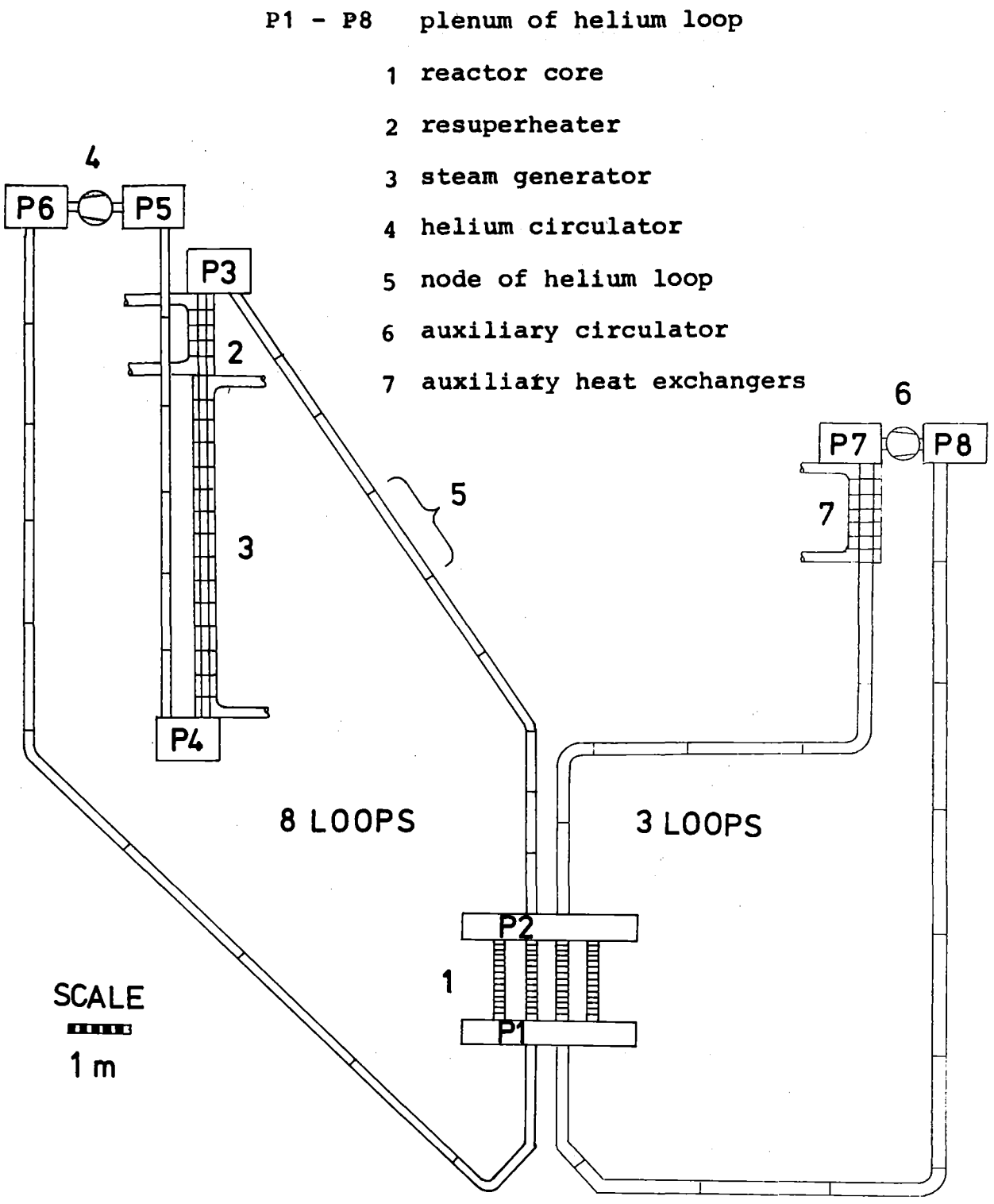


Fig. 4.0 PHAETON 2 model of the 1000 MW reactor with standing core, 4 core links, elevated steam generators, and elevated auxiliary heat exchangers.

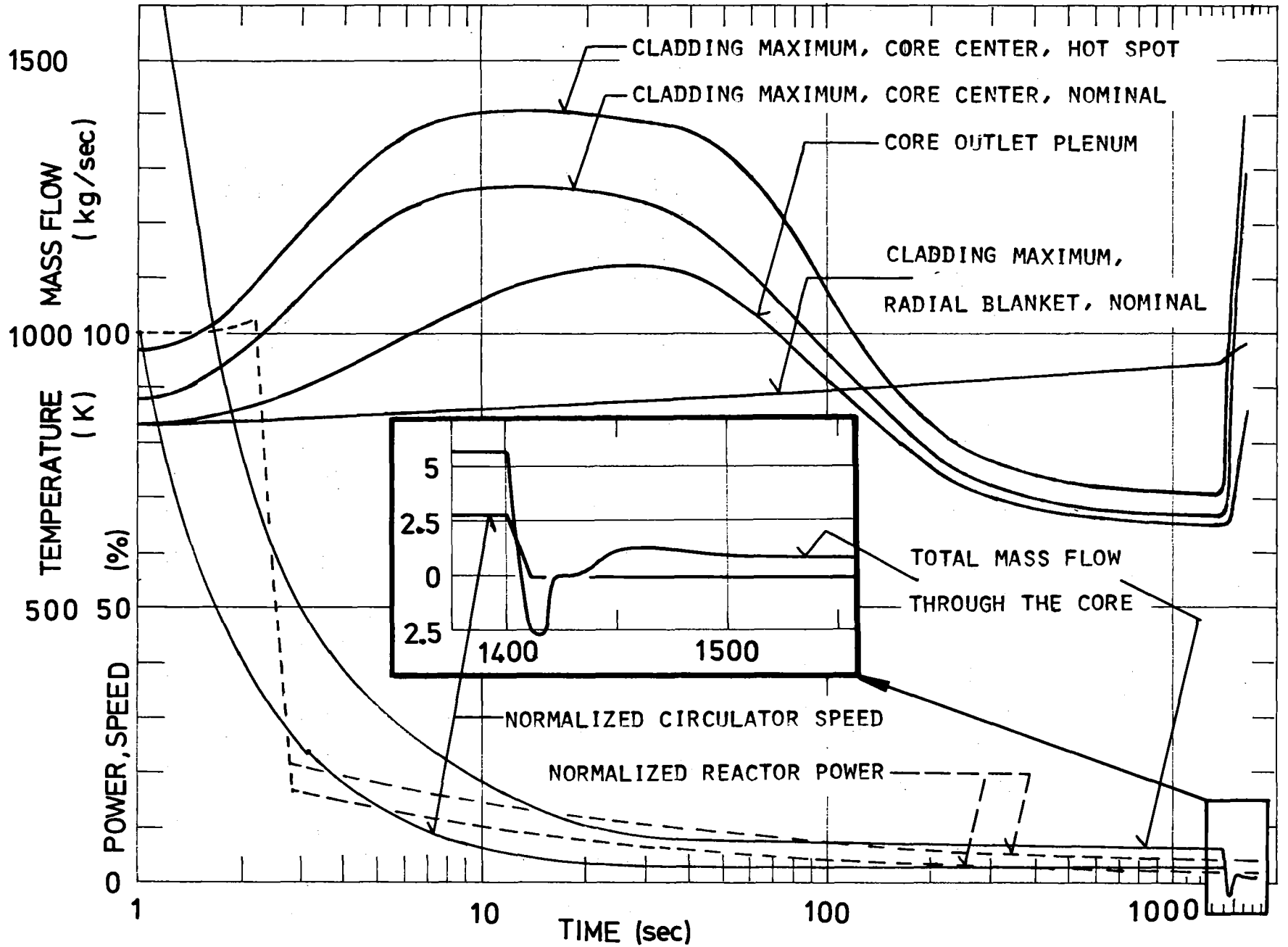


Fig. 4.1 Flow coast-down accident for the model of fig. 4.0

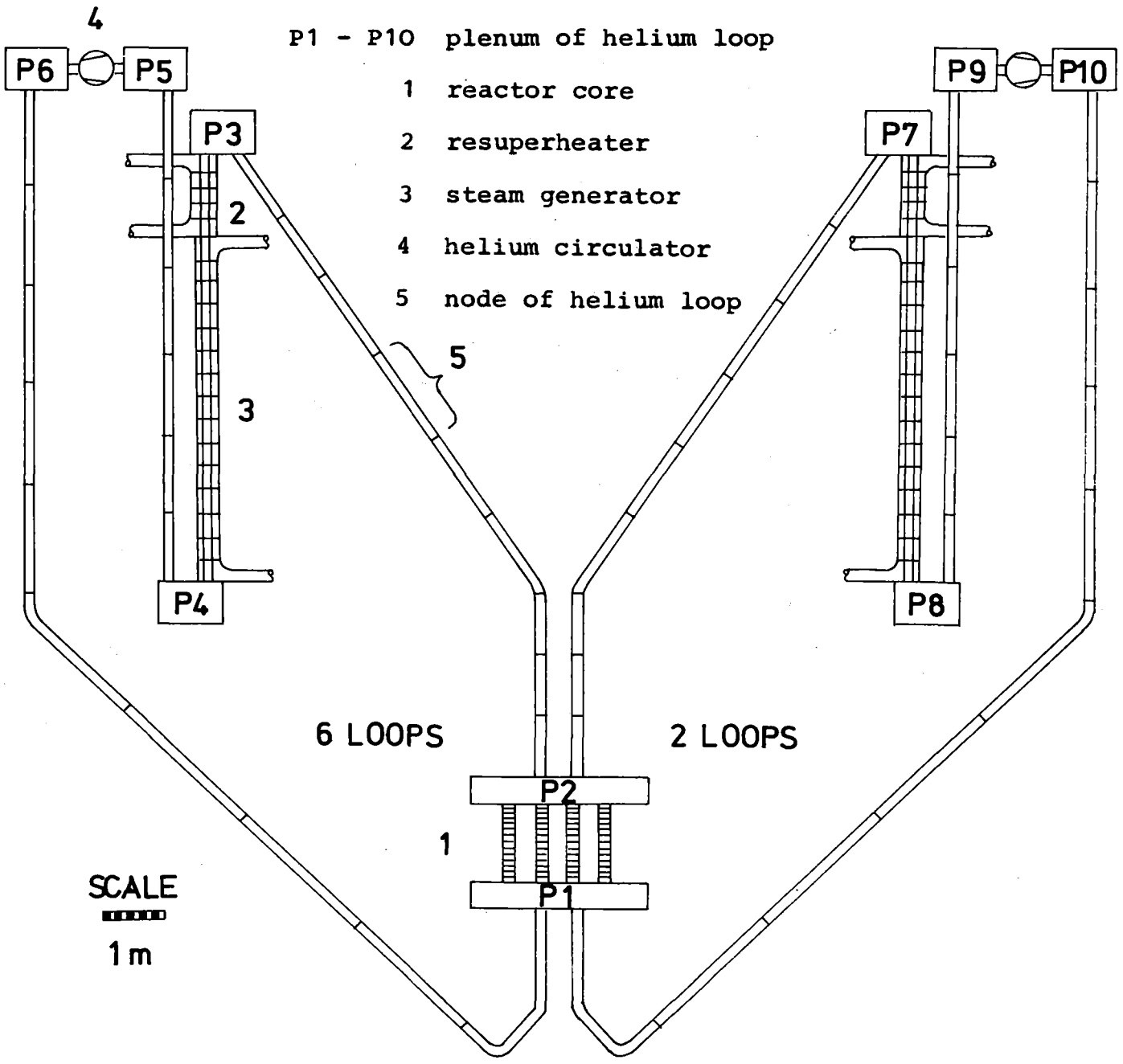


Fig. 5.0 PHAETON 2 model of the 1000 MW reactor with standing core, 4 core links, and two parallel elevated steam generators

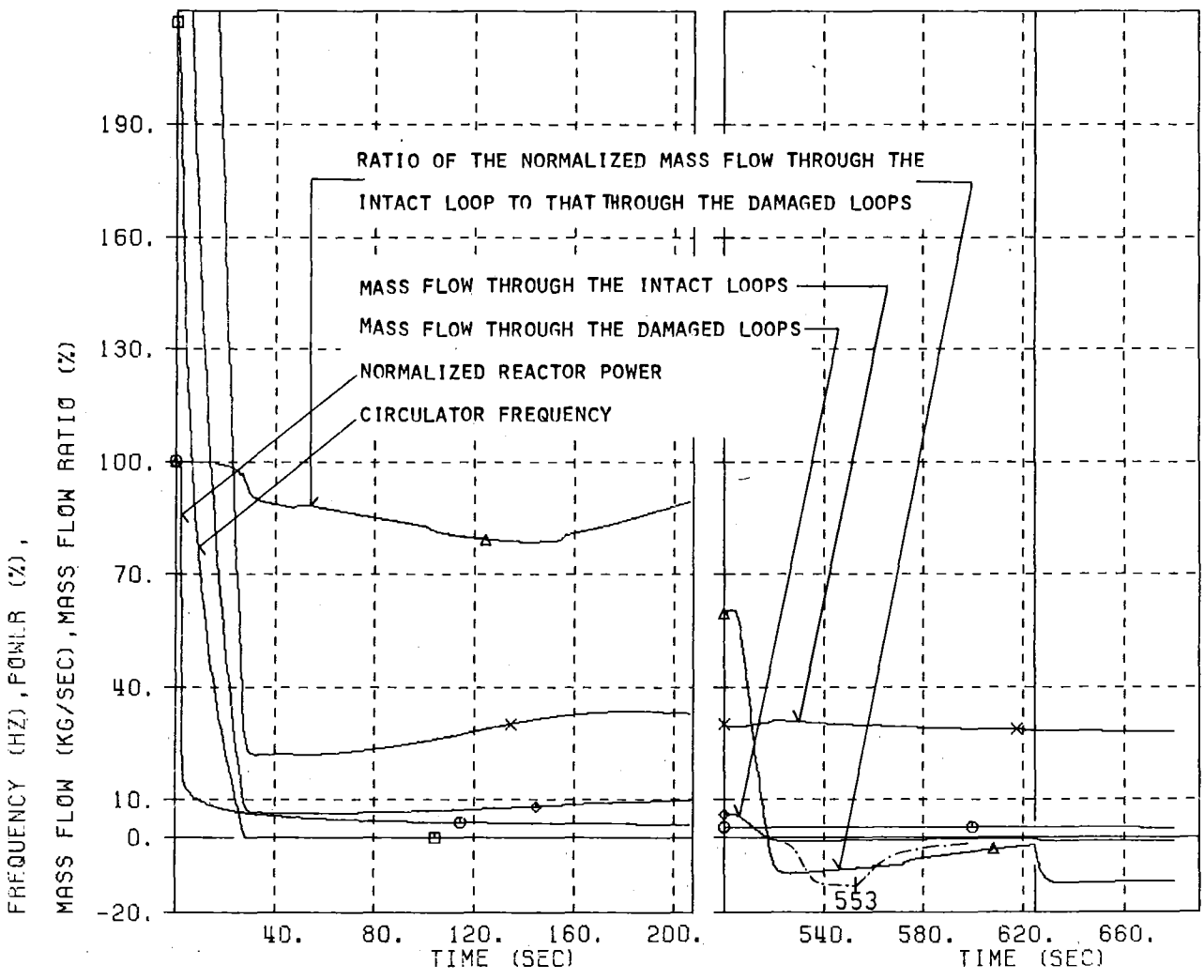


**Fig. 5.1 Flow coast-down accident for the model of fig. 5.0**

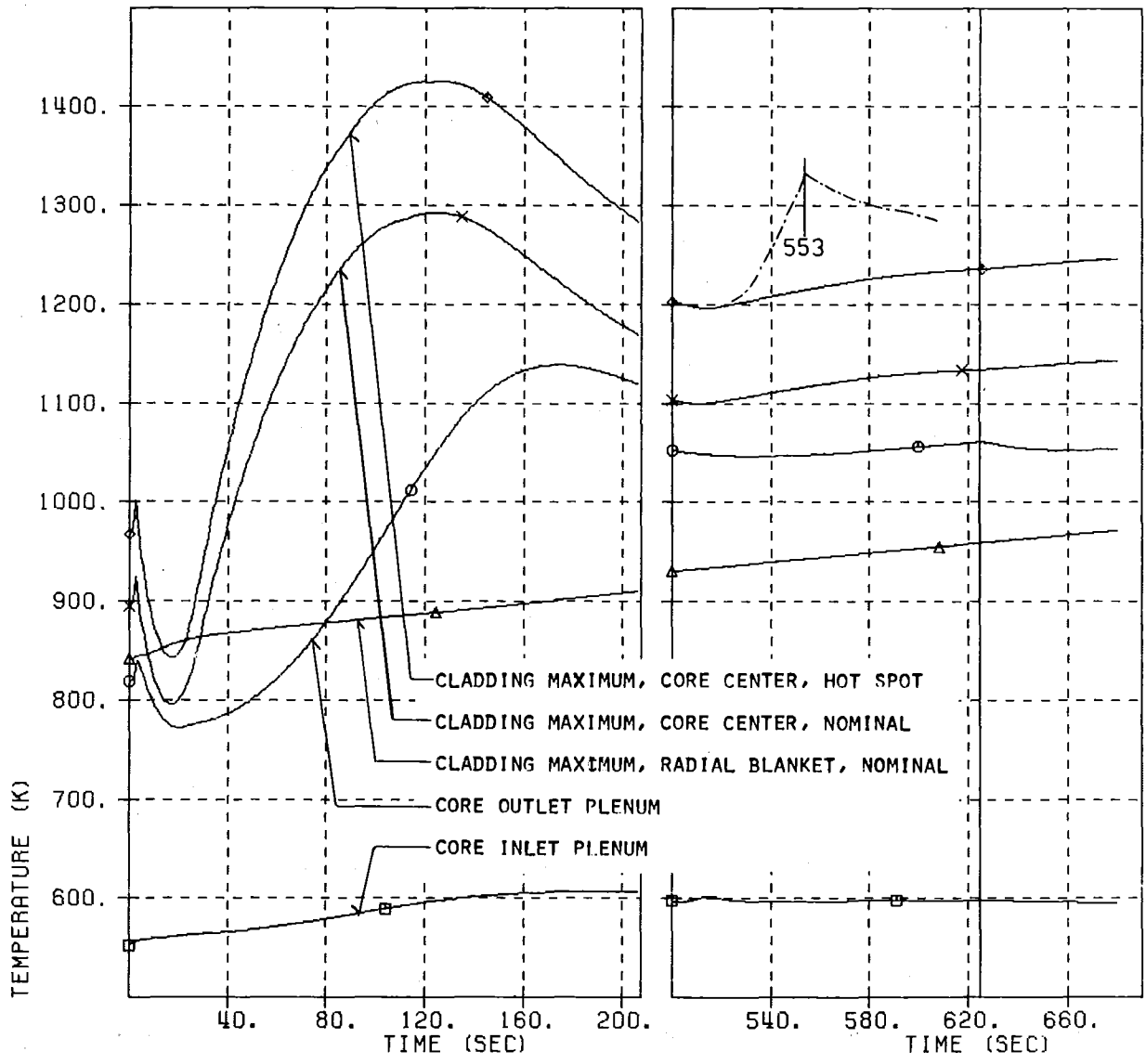


**Fig. 5.2 Flow coast-down accident for the model of fig. 5.0**

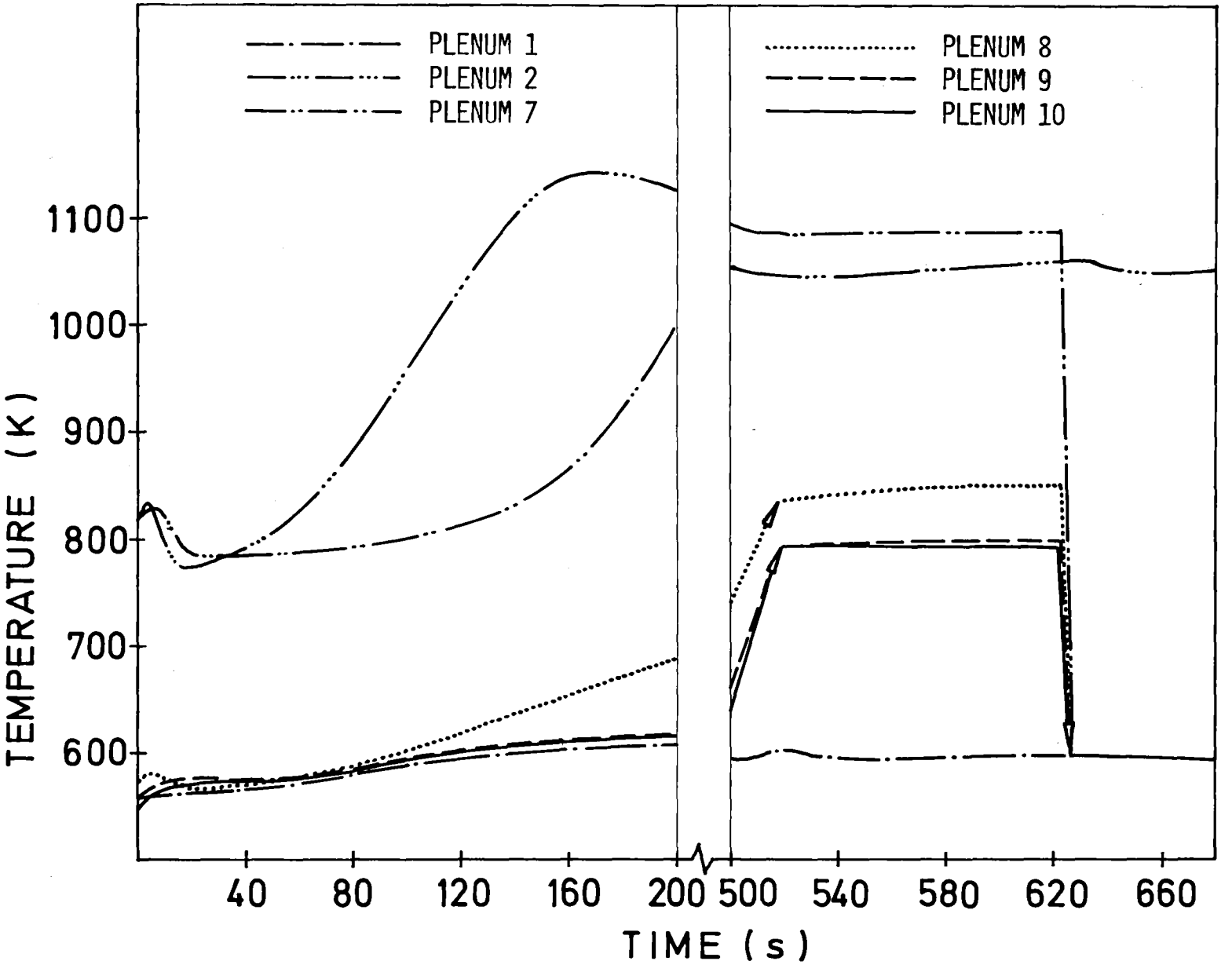


Fig. 5.3 Flow coast-down accident for the model of fig. 5.0

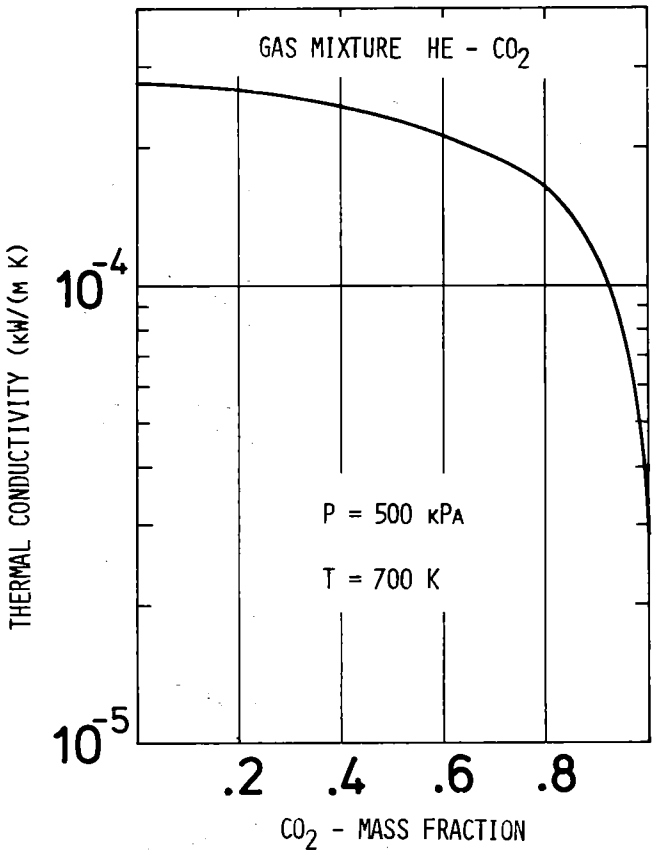


Fig. 6.3 Thermal conductivity of a He-$CO_2$ gas mixture

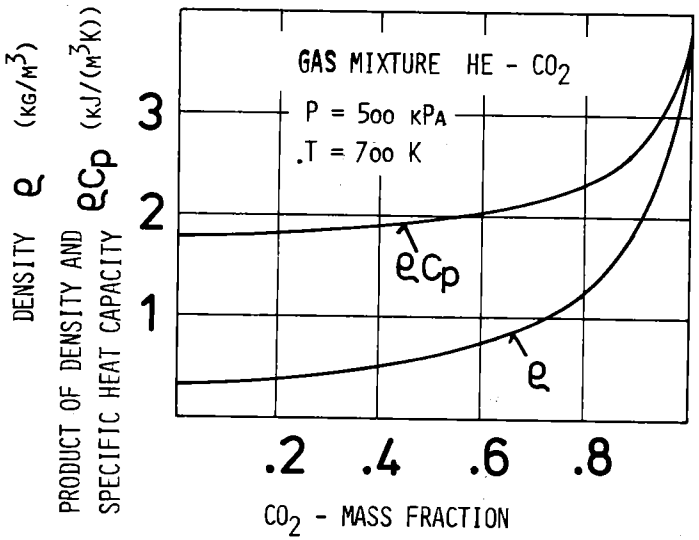


Fig. 6.1 Density and heat capacity of a He-$CO_2$ gas mixture

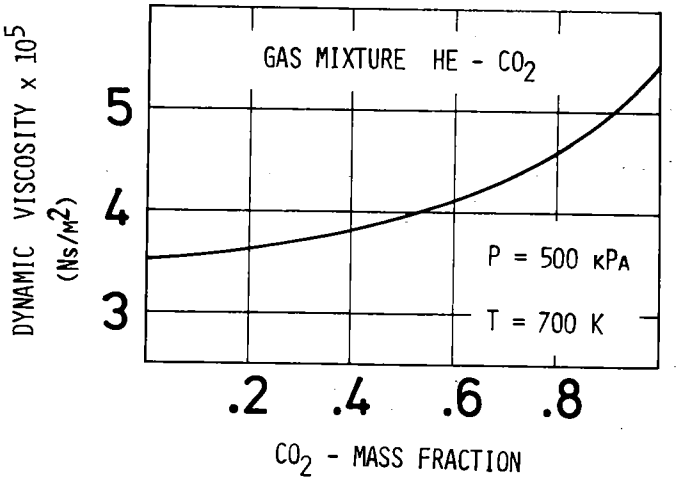


Fig. 6.2 Viscosity of a He-$CO_2$ gas mixture

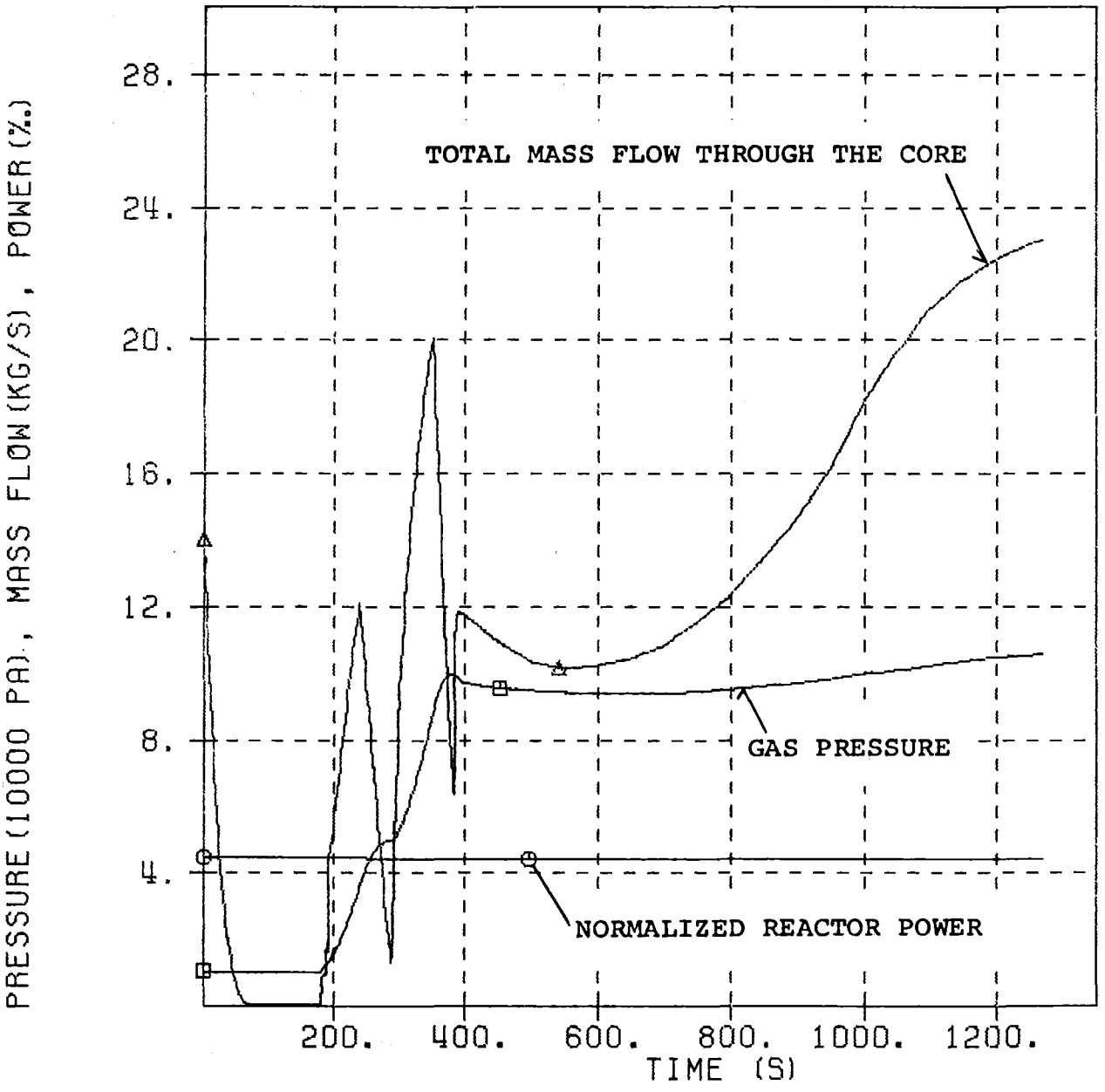


Fig. 6.4: Flow coast-down accident during refueling with $CO_2$-supply

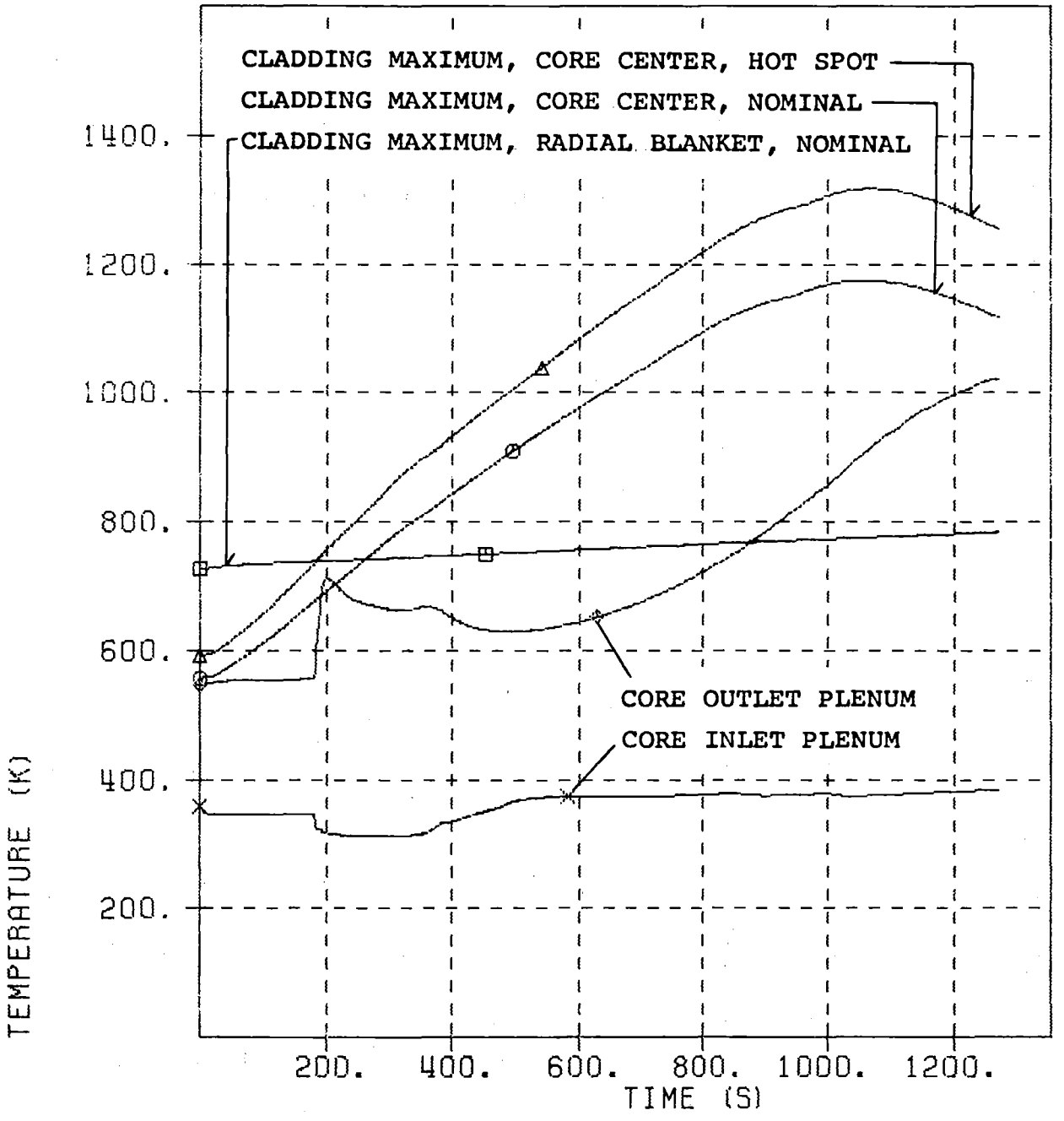


Fig. 6.5: Flow coast-down accident during refueling with $CO_2$-supply